Domain decomposition method based on One-Way approaches for sound propagation in a partially lined duct

Maelys Ruello, Clément Rudel, Sébastien Pernet, Jean-Philippe Brazier

Domain decomposition method based on One-Way approaches for sound propagation in a partially lined duct

Maëlys Ruello[a,*], Clément Rudel[a], Sébastien Pernet[a], Jean-Philippe Brazier[b]

[a] *DTIS, ONERA, Université de Toulouse, 31000, Toulouse, France*
[b] *DMPE, ONERA, Université de Toulouse, 31000, Toulouse, France*

Abstract

A numerical factorization method of the unidirectional propagation operators induced by the linearized Euler and Navier-Stokes equations is performed to construct a new One-Way approach to compute the sound radiation in a partially lined duct. The complex phenomena of reflection and transmission of incident waves originating from discontinuities in the duct wall are accurately taken into account by an iterative domain decomposition method. Furthermore, the proposed factorization approach allows both the derivation of the lined duct scattering matrix and an in-depth understanding of the impact of the acoustic liner on left- and right-going waves coming from a transmission or a reflection. Finally, the efficiency of the numerical method is shown based on a classical benchmark with two types of baseflows (laminar and turbulent Poiseuille flows) and by comparison with other numerical and experimental results. An unstable surface mode is observed at 1000 Hz, and we find good agreement with experimental data for the turbulent mean flow associated with the One-Way Navier-Stokes equations.

Keywords: One-Way approaches, Hyperbolic equations, Domain decomposition method, Acoustic Liners, Hydrodynamic Instability
2020 MSC: 35L02,
2020 MSC: 65N22,
2020 MSC: 65N55,
2020 MSC: 76Q05

1. Introduction

Acoustic liners are used in a wide variety of duct configurations to decrease the sound level produced by a wave propagating across a duct. This surface treatment has been used for many years in the aeronautical domain to decrease the sound produced by aircraft engines which is, nowadays, a major issue of the commercial aviation and therefore, an active field of study. The development of such treatment requires many numerical simulations and experimental measurements in order to better understand the phenomena appearing inside the duct and their underlying mechanisms.

*Corresponding author
Email addresses: maelys.ruello@onera.fr (Maëlys Ruello), crudel30@gmail.com (Clément Rudel), sebastien.pernet@onera.fr (Sébastien Pernet), jean-philippe.brazier@onera.fr (Jean-Philippe Brazier)

The setup classically used for the numerical study of such configurations is a duct, with a rectangular or round section, with walls partially covered with an acoustic liner. The main challenge in this type of simulation is to model accurately the effect of the liner on the incident wave propagating across the duct. In fact, an acoustic liner generally consists of a network of honeycomb cavities on a rigid backing plate and beneath a resistive plate, which may be a perforated plate or a wire-mesh fabric. To avoid calculating all the physical phenomena taking place in the liner, an impedance boundary condition is usually imposed on the liner wall. The porous nature of this absorbing material creates a discontinuity in boundary conditions, leading to reflection and refraction of waves inside the duct, with non-negligible effects on the results obtained. Moreover, the flow present in the duct adds some complexity in the model used, since it affects the kind of waves propagated and can lead to the appearance of instabilities.

To compute this kind of configurations, linear models are used since the mechanisms involved in the range of frequency, velocity, and energy generally studied are mainly linear. This assumption of linearity allows using computational methods that are far less costly than Direct Numerical Simulations [1] that would be required instead. A time domain resolution of linearized Euler or Navier-Stokes equations has already shown good results [2] and takes naturally into account the reflection and refraction of waves. However, the formulation of the equations requires the use of impedance boundary conditions in the time domain [3, 4, 5], which can be quite complex to impose. The issue of imposing correct inlet and outlet boundary conditions is also present, with the use of perfectly matched layers [6] for example, in order to avoid unwanted waves propagating back in the computational domain. Similar systems of equations can also be solved in the frequency domain, making it much easier to impose the impedance boundary condition. But the issue of non-reflecting boundary conditions remains present, and this type of resolution requires solving large linear systems, which can lead to huge CPU and memory resources.

Another standard approach is to use a modal decomposition of the propagation problem, which consists in the decomposition of the propagating waves as a sum of modes in the frequency domain. These kinds of approaches are also frequently used in other domains of aeroacoustics such as jet noise or boundary layer stability studies. For such applications as the partially lined duct characterization, they are, in general, coupled to mode matching techniques [7] or to a Wiener-Hopf solution [8]. However, these methods are either limited by hypotheses for their fields of application or by a costly decomposition in modes of the propagation operators.

An alternative solution to these limitations is to use One-Way approaches, which consist of decoupling the waves propagating in one direction and the other, to keep only the part of interest. One-Way approaches have been used for fifty years in diverse fields such as geophysics [9], acoustics, or electromagnetism. This method has the advantage of being less computationally costly than "exact methods" and has a wider range of applications than Parabolized Stability Equations [10]. The existence and construction of such decoupling has been known since the work of M. Taylor [11] and his factorization method based on a microlocal analysis of hyperbolic problems [12]. Nevertheless, the analytical nature of this type of method, using symbolic calculus and pseudo-differential operators, makes its development unaffordable for complex systems such as the Euler and Navier-Stokes equations.

Recently, T. Colonius' team at Caltech [13, 14, 15] bypassed this difficulty for fluid mechanics problems by using a non-reflecting boundary condition [16, 17, 18, 19], that permits to avoid complicated analytical developments of the equations. However, this method is limited by a hypothesis of slow variation in the baseflow along the propagation direction, which includes also any variation in the transverse boundary conditions. A derivation of these One-Way equations

has been presented in [20] and applied to the problem of a partially lined duct in [21]. This method is based on the full numerical construction of the projection operators that are needed to take into account the reflection and transmission of waves across any variation. In this paper, the method of resolution is applied to the same type of configuration but with a different type of acoustic liner (CT57) presenting an instability at 1000 Hz, with an emphasis on the decomposition feature of the waves naturally obtained with these equations and also an extension to linearized Navier-Stokes equations.

In Section 2, we propose a numerical One-Way factorization of the propagation operator for linear hyperbolic problems. The method of domain decomposition is explained in Section 3.1 while the computation of the reflection and transmission of waves at the boundary discontinuities is developed in Section 3.2. Finally, we will illustrate this approach with some numerical results for an acoustic liner contained in a duct for two types of baseflows and for One-Way Euler (OWE) and One-Way Navier-Stokes (OWNS) equations in Section 4. The results will be compared to other numerical simulations and experimental data.

2. Numerical One-Way factorization of the propagation operator for hyperbolic problems

To present the construction of the numerical One-Way factorization of a unidirectional propagation operator, we use the following system of hyperbolic linear differential equations:

$$\frac{\partial q}{\partial t} + A(x,y)\frac{\partial q}{\partial x} + B_y(x,y)\frac{\partial q}{\partial y} + B_{yy}(x,y)\frac{\partial^2 q}{\partial y^2} + C(x,y)q = 0. \tag{1}$$

We then choose a preferred direction, here x, and we first apply a Fourier-Laplace transform in time to pass the system (1) into the frequency domain. As we are only interested in the system's stationary behavior, we will assume zero initial conditions. The Fourier transform of the variable q describing the perturbation will be written $q = \widetilde{q}e^{-i\omega t}$, with ω the angular frequency. We next process as in [14] by isolating the term $\frac{\partial}{\partial x}$ and by performing a first discretization in the transverse direction y using a numerical approximation such as a compact high-order finite difference scheme, for example a 4$^{\text{th}}$ to 6$^{\text{th}}$ order finite difference compact scheme [22].

By using a bold notation to represent the semi-discrete counterpart of the variables, Eq. (1) then leads to:

$$\mathbf{A}(x)\frac{\mathrm{d}\widetilde{\mathbf{q}}}{\mathrm{d}x} = \left(i\omega\mathbf{I} - \mathbf{B}_y\mathbf{D}_y - \mathbf{B}_{yy}\mathbf{D}_{yy} - \mathbf{C}\right)\widetilde{\mathbf{q}} := \mathbf{B}(x)\widetilde{\mathbf{q}}, \tag{2}$$

with $\mathbf{D}_y$ and $\mathbf{D}_{yy}$ the first and second order discrete derivative operators in y-variable.

The equation (1) is assumed to be hyperbolic, the matrix $A(x,y)$ is then necessarily $\mathbb{R}$-diagonalizable for each value of x i.e., the eigenvalues are real. Since $\mathbf{A}$ is the semi-discretized version of A, the same property holds, i.e., $\mathbf{A}$ has N real eigenvalues which correspond to N_+ positive, N_- negative and N_0 null eigenvalues. Consequently, the matrix $\mathbf{A}$ being diagonalizable, there is an invertible transformation matrix $\mathbf{T}$ such that:

$$\mathbf{T}^{-1}\mathbf{A}\mathbf{T} = \widetilde{\mathbf{A}} = \begin{pmatrix} \widetilde{\mathbf{A}}_{++} & \mathbf{0} & \mathbf{0} \\ \mathbf{0} & \widetilde{\mathbf{A}}_{--} & \mathbf{0} \\ \mathbf{0} & \mathbf{0} & \mathbf{0}_{N_0\times N_0} \end{pmatrix}, \tag{3}$$

with $\widetilde{\mathbf{A}}$ being the diagonal matrix containing all the eigenvalues of $\mathbf{A}$, and $\widetilde{\mathbf{A}}_{++} \in \mathbb{R}^{N_+\times N_+}$ and $\widetilde{\mathbf{A}}_{--} \in \mathbb{R}^{N_-\times N_-}$ being the two diagonal matrices containing positive and negative eigenvalues, respectively.

For the sake of clarity of the presentation, we now assume that $N_0 = 0$ and, consequently, $\widetilde{\mathbf{A}}$ is an invertible matrix. The case $N_0 \neq 0$ can be easily solved by proceeding to a reduction of the system by eliminating the linear dependencies induced by these null eigenvalues. This kind of situation appears for example when the mean flow vanishes at the wall boundaries.

We now perform the following variable change $\boldsymbol{\phi} = \mathbf{T}^{-1}\widetilde{\mathbf{q}}$, called the characteristic variables, and we get the new system of equations:

$$\frac{\mathrm{d}\boldsymbol{\phi}}{\mathrm{d}x} = \left(\widetilde{\mathbf{A}}^{-1}\mathbf{T}^{-1}\mathbf{B}\mathbf{T} - \mathbf{T}^{-1}\frac{\mathrm{d}\mathbf{T}}{\mathrm{d}x}\right)\boldsymbol{\phi} := \mathbf{M}(x)\boldsymbol{\phi}, \tag{4}$$

where the matrix $\mathbf{M}$ is called the propagation operator along the preferred direction x.

From the previous decomposition of $\widetilde{\mathbf{A}}$ into positive and negative eigenvalues, we can do the same for the propagation operator and the vector $\boldsymbol{\phi}$. Equation (4) can be written as:

$$\frac{\mathrm{d}}{\mathrm{d}x}\begin{pmatrix}\boldsymbol{\phi}_+\\ \boldsymbol{\phi}_-\end{pmatrix} = \begin{pmatrix}\mathbf{M}_{++} & \mathbf{M}_{+-}\\ \mathbf{M}_{-+} & \mathbf{M}_{--}\end{pmatrix}\begin{pmatrix}\boldsymbol{\phi}_+\\ \boldsymbol{\phi}_-\end{pmatrix}, \tag{5}$$

the first index designating the number of rows (N_+ or N_-) and the second, the number of columns in the block matrix.

The construction of One-Way methods requires identifying left and right-going modes contained in the propagation operator $\mathbf{M}$. A natural way to do so is to diagonalize $\mathbf{M}$ and analyze the behavior of the eigenvalues to determine different categories of modes, by using Briggs' criterion [23], for example. However, this approach is generally costly in terms of computational resources, largely because $\mathbf{M}$ depends on x. To bypass this problem, we propose to construct a new factorization of the propagation operator based on the concept of high-order non-reflective boundary conditions. The starting point of this method is based on the following observation: a "strict" diagonalization of $\mathbf{M}$ is not necessary to complete a One-Way decoupling, and the knowledge of a family of vectors which generates the invariant spaces is sufficient.

In this section, we revisit in a more theoretically framework the construction method of the One-Way equations using a purely numerical factorization that we have proposed in the seminal paper [20]. In the first part, a characterization technique of the right and left invariant spaces associated to the right and left-going modes, respectively, is presented. It is based on the application of two non-reflective boundary conditions [19] which allows computing two sets of N_+ and N_- vectors generating vector spaces for extraction according to the direction of wave propagation. In the second part, these "pseudo-eigenvectors" enable us to construct a matrix of the same nature as the left eigenvectors' matrix of $\mathbf{M}$. Finally, from this matrix, we get a new factorization of the propagation operator and new One-Way equations to solve (2).

2.1. Identification of the left and right invariant spaces using non-reflecting boundary conditions

We are interested in the identification of the two invariant spaces of the propagation operator $\mathbf{M}(x)$ for a fixed value of x. They correspond to the right and left invariant spaces corresponding to the generated spaces by the right and left-going modes, respectively. We know that they are of size N_+ and N_-, respectively. In this section, we are using two non-reflective boundary conditions of type (6), built from the same set of given parameters $\left(\beta_\pm^j\right)_j$, in order to approximate these two spaces. Thus, for each value of x, it is shown that it is not only possible to access information necessary to wave propagation to the right and to the left, but also to get a complete separation of this information. This separation, which is the basis for One-Way equations decoupling, is

necessary to their good local resolution. The following Subsection 2.1.1 concerns the subject of left invariant space using a non-reflective boundary condition of right type (i.e., which allows suppressing left-going waves and keeping right-going waves). Subsection 2.1.2 is using the same reasoning in the case of right invariant space.

2.1.1. Approximation of the left invariant space

The purely numerical construction method of the One-Way equations is based on the use of a non-reflecting boundary condition, which avoids the construction of a complete diagonalization of the propagation operator $\mathbf{M}$. This type of boundary condition was first introduced by Higdon [17] and then derived in a high-order version by Givoli & Neta [18]. Its application to hyperbolic systems, such as those of Euler or Navier-Stokes, can be found in an article from Hagstrom & Warburton [19].

This condition preserves information propagating in one direction and removes the rest when solving the equations. However, in order to increase the range of application of such equations, the information propagating in both directions must be preserved. In addition, it needs to be filtered so that it can be separated, and a special treatment can be applied to each of its components. The idea is therefore to apply this type of non-reflective condition in both directions of propagation to determine the terms (in discretized form) responsible for wave propagation in one direction or the other.

We start by recalling the approximation of the One-Way equations given by Towne & Colonius in various publications [14, 15, 13] is given by the following expression:

$$\begin{cases} \dfrac{\mathrm{d}\boldsymbol{\phi}_+}{\mathrm{d}x} = \mathbf{M}_{++}\boldsymbol{\phi}_+ + \mathbf{M}_{+-}\boldsymbol{\phi}_-, \\ (\mathbf{M} - i\beta_+^j\mathbf{I})\boldsymbol{\phi}^j = (\mathbf{M} - i\beta_+^j\mathbf{I})\boldsymbol{\phi}^{j+1},\ j = 0, ..., N_\beta - 1 \\ \boldsymbol{\phi}_-^{N_\beta} = \mathbf{0}, \\ \boldsymbol{\phi}(x_0) \text{ given }, \end{cases} \tag{6}$$

with x_0 the abscissa at the inlet of the computational domain where a boundary condition is applied.

The system (6) given by Towne & Colonius can be rewritten under the following compact form as:

$$\begin{cases} \dfrac{\mathrm{d}\boldsymbol{\phi}_+}{\mathrm{d}x} = \mathbf{M}_{++}\boldsymbol{\phi}_+ + \mathbf{M}_{+-}\boldsymbol{\phi}_-, \\ \begin{pmatrix} \boldsymbol{\phi}_+^{N_\beta} \\ \mathbf{0} \end{pmatrix} = \mathbf{Z}^{r,N_\beta} \begin{pmatrix} \boldsymbol{\phi}_+ \\ \boldsymbol{\phi}_- \end{pmatrix}. \end{cases} \tag{7}$$

which allows introducing the right non-reflection matrix $\mathbf{Z}^{r,N_\beta}$, obtained by recurrence:

$$\mathbf{Z}^{r,N_\beta} = \prod_{j=0}^{N_\beta-1} (\mathbf{M} - i\beta_-^j\mathbf{I})^{-1}(\mathbf{M} - i\beta_+^j\mathbf{I}). \tag{8}$$

This matrix is the starting point of our identification technique because if the set of parameter $\left(\beta_\pm^j\right)_j$ is well-chosen, the action of this matrix is both to "neutralize" the left-going modes and to preserve the right-going ones.

Nevertheless, to ensure the robustness of the method, it is crucial to introduce the following "preconditioned" version $\widetilde{\mathbf{Z}}^{r,N_\beta}$ of the matrix $\mathbf{Z}^{r,N_\beta}$:

$$\widetilde{\mathbf{Z}}^{r,N_\beta} = \begin{pmatrix} \mathbf{I}_{++} & \left(\mathbf{Z}_{++}^{r,N_\beta}\right)^{-1} \mathbf{Z}_{+-}^{r,N_\beta} \\ \left(\mathbf{Z}_{--}^{r,N_\beta}\right)^{-1} \mathbf{Z}_{-+}^{r,N_\beta} & \mathbf{I}_{--} \end{pmatrix}. \tag{9}$$

The behavior of $\widetilde{\mathbf{Z}}^{r,N_\beta}$ strongly depends on the choice of a family of parameters $(\beta_\pm^j)_{j\in\mathbb{N}}$ with respect to the location of the left- and right-going modes of $\mathbf{M}$ in the complex plane. To formalize these constraints, we adopt the following definition:

Definition 1. *A family of parameters $(\beta_\pm^j)_{j\in\mathbb{N}}$ is said to be adapted to the propagation operator $\mathbf{M}(x)$ if and only if: for all eigenvalues $i\alpha_+$ and $i\alpha_-$ of $\mathbf{M}(x)$, associated to a right- and left-going mode, respectively, we have the following property:*

$$\begin{cases} \lim\limits_{N_\beta\to+\infty} \prod\limits_{j=0}^{N_\beta-1} \left|\dfrac{\alpha_+ - \beta_+^j}{\alpha_+ - \beta_-^j}\right| = 0, \\ \lim\limits_{N_\beta\to+\infty} \prod\limits_{j=0}^{N_\beta-1} \left|\dfrac{\alpha_- - \beta_+^j}{\alpha_- - \beta_-^j}\right| = +\infty. \end{cases} \tag{10}$$

We suppose for the rest of this part that the family of parameters $(\beta_\pm^j)_{j\in\mathbb{N}}$ is adapted to the propagation operator. We then can prove the convergence result:

Theorem 1. *Let $(\beta_\pm^j)_{j\in\mathbb{N}}$ be a family of parameters adapted to the propagation operator $\mathbf{M}$ at the point x whose a diagonalization is written $\mathbf{M} = \mathbf{VDU}$. We then have the two following results:*

i. The matrix subsequence $\widetilde{\mathbf{Z}}_{-+}^{r,N_\beta}$ admits a limit noted $\widetilde{\mathbf{Z}}_{-+}^{r}$ defined by:

$$\lim_{N_\beta\to+\infty} \widetilde{\mathbf{Z}}_{-+}^{r,N_\beta} = \widetilde{\mathbf{Z}}_{-+}^{r} = \mathbf{U}_{--}^{-1}\mathbf{U}_{-+}. \tag{11}$$

ii. We have the following identity:

$$\begin{pmatrix} \widetilde{\mathbf{Z}}_{-+}^{r} & \widetilde{\mathbf{Z}}_{--}^{r} \end{pmatrix} \mathbf{M} = \left(\mathbf{U}_{--}^{-1}\mathbf{D}_{--}\mathbf{U}_{--}\right) \begin{pmatrix} \widetilde{\mathbf{Z}}_{-+}^{r} & \widetilde{\mathbf{Z}}_{--}^{r} \end{pmatrix}, \tag{12}$$

In addition, let $\mathcal{S}^l := Span\left\{\mathbf{U}_{i,*} \in \mathbb{C}^{N_+ + N_-} | i = N_+ + 1, ..., N_+ + N_-\right\}$ be the left invariant space generated by the left eigenvectors of $\mathbf{M}$. Then the space

$$\widetilde{\mathcal{S}}^l := Span\left\{\widetilde{\mathbf{Z}}_{i,*}^{r} \in \mathbb{C}^{N_+ + N_-} | i = N_+ + 1, ..., N_+ + N_-\right\} \tag{13}$$

verifies the left invariance property: $\forall\ \widetilde{\mathbf{W}} \in \widetilde{\mathcal{S}}^l$, we have:

$$\widetilde{\mathbf{W}}\mathbf{M} \ \in Span\left\{\mathbf{U}_{--}^{-1}\mathbf{W} :\ \forall\ \mathbf{W} \in \mathcal{S}^l\right\}, \tag{14}$$

and $\forall\ \mathbf{W} \in \mathcal{S}^l$, we have:

$$\mathbf{W}\mathbf{M} \ \in Span\left\{\mathbf{U}_{--}\widetilde{\mathbf{W}} :\ \forall\ \widetilde{\mathbf{W}} \in \widetilde{\mathcal{S}}^l\right\}. \tag{15}$$

Proof. We first demonstrate 1. To do so, we use the fact that $\mathbf{Z}^{r,N_\beta}$ possesses the same eigenvalues as $\mathbf{M}$, associated to the eigenvalues matrices $\mathbf{R}_{++}^{r,N_\beta}$ and $\mathbf{R}_{--}^{r,N_\beta}$ i.e.,

$$\mathbf{Z}^{r,N_\beta}\mathbf{V} = \mathbf{V}\begin{pmatrix} \mathbf{R}_{++}^{r,N_\beta} & \mathbf{0} \\ \mathbf{0} & \mathbf{R}_{--}^{r,N_\beta} \end{pmatrix}. \tag{16}$$

with $\mathbf{R}_{++}^{r,N_\beta}$ and $\mathbf{R}_{--}^{r,N_\beta}$ two diagonal matrices whose k^{th} terms are defined by:

$$\mathbf{R}_{++,k}^{r,N_\beta} = \prod_{j=0}^{N_\beta} \frac{\alpha_{+,k} - \beta_+^j}{\alpha_{+,k} - \beta_-^j}, \tag{17}$$

and

$$\mathbf{R}_{--,k}^{r,N_\beta} = \prod_{j=0}^{N_\beta} \frac{\alpha_{-,k} - \beta_+^j}{\alpha_{-,k} - \beta_-^j}. \tag{18}$$

By doing block products, we have in particular the following relation:

$$\mathbf{Z}_{-+}^{r,N_\beta}\mathbf{V}_{++} + \mathbf{Z}_{--}^{r,N_\beta}\mathbf{V}_{--} = \mathbf{V}_{-+}\mathbf{R}_{++}^{r,N_\beta} \tag{19}$$

that can be rewritten as:

$$(\mathbf{Z}_{--}^{r,N_\beta})^{-1}\mathbf{Z}_{-+}^{r,N_\beta} + \mathbf{V}_{-+}(\mathbf{V}_{++})^{-1} = (\mathbf{Z}_{--}^{r,N_\beta})^{-1}\mathbf{V}_{-+}\mathbf{R}_{++}^{r,N_\beta}(\mathbf{V}_{++})^{-1} \tag{20}$$

By reusing the fact that $\mathbf{Z}^{r,N_\beta}$ has the same eigenvalues as $\mathbf{M}$, we deduce that:

$$\mathbf{Z}_{--}^{r,N_\beta} = \mathbf{V}_{-+}\mathbf{R}_{++}^{r,N_\beta}\mathbf{U}_{+-} + \mathbf{V}_{--}\mathbf{R}_{--}^{r,N_\beta}\mathbf{U}_{--}. \tag{21}$$

The hypothesis made on the family of parameters $(\beta_\pm^j)_{j\in\mathbb{N}}$ allows us to pass to the limit and to deduce the following identity:

$$\widetilde{\mathbf{Z}}_{-+}^{r} + \mathbf{V}_{-+}(\mathbf{V}_{++})^{-1} = \mathbf{0}, \tag{22}$$

as we have $\lim_{N_\beta\to+\infty} \|\mathbf{R}_{++}^{r,N_\beta}\| = 0$ and $\lim_{N_\beta\to+\infty} \|(\mathbf{Z}_{--}^{r,N_\beta})^{-1}\| = 0$ because $\lim_{N_\beta\to+\infty} \|\mathbf{R}_{--}^{r,N_\beta}\| = +\infty$. We then use the $\mathbf{UV} = \mathbf{I}$ identity to find the next relation:

$$\mathbf{U}_{-+}\mathbf{V}_{++} + \mathbf{U}_{--}\mathbf{V}_{-+} = \mathbf{0}, \tag{23}$$

which can also be written as:

$$\mathbf{V}_{-+}(\mathbf{V}_{++})^{-1} = -(\mathbf{U}_{--})^{-1}\mathbf{U}_{-+}. \tag{24}$$

By combining (22) and (24), we immediately get 1.

We now demonstrate 1. The first part comes immediately with the 1 result. Indeed, we have:

$$\begin{aligned} \left(\widetilde{\mathbf{Z}}_{-+}^{r}\widetilde{\mathbf{Z}}_{--}^{r}\right)\mathbf{M} &= \left(\mathbf{U}_{--}^{-1}\mathbf{U}_{-+}\mathbf{I}\right)\mathbf{M} \\ &= \mathbf{U}_{--}^{-1}\left(\mathbf{U}_{-+}\mathbf{U}_{--}\right)\mathbf{M} \\ &= \mathbf{U}_{--}^{-1}\mathbf{D}_{--}\left(\mathbf{U}_{-+}\mathbf{U}_{--}\right) \\ &= \mathbf{U}_{--}^{-1}\mathbf{D}_{--}\mathbf{U}_{--}\left(\mathbf{U}_{--}^{-1}\mathbf{U}_{-+}\mathbf{I}\right) \\ &= \left(\mathbf{U}_{--}^{-1}\mathbf{D}_{--}\mathbf{U}_{--}\right)\left(\widetilde{\mathbf{Z}}_{-+}^{r}\widetilde{\mathbf{Z}}_{--}^{r}\right) \end{aligned} \tag{25}$$

To show the invariance property, we exploit the previous identity. Let $\widetilde{\mathbf{W}} \in \widetilde{\mathcal{S}}^l$. $\widetilde{\mathbf{W}}$ can be written as $\widetilde{\mathbf{W}} = \widetilde{\Lambda}_{--}\left(\widetilde{\mathbf{Z}}^r_{-+}\widetilde{\mathbf{Z}}^r_{--}\right)$ with $\widetilde{\Lambda}_{--}$ a diagonal matrix of size N_-. We then have:

$$\begin{aligned}\widetilde{\mathbf{W}}\mathbf{M} &= \widetilde{\Lambda}_{--}\left(\widetilde{\mathbf{Z}}^r_{-+}\widetilde{\mathbf{Z}}^r_{--}\right)\mathbf{M} \\ &= \widetilde{\Lambda}_{--}\left(\mathbf{U}^{-1}_{--}\mathbf{D}_{--}\mathbf{U}_{--}\right)\left(\widetilde{\mathbf{Z}}^r_{-+}\widetilde{\mathbf{Z}}^r_{--}\right) \\ &= \widetilde{\Lambda}_{--}\mathbf{U}^{-1}_{--}\underbrace{\mathbf{D}_{--}\left(\mathbf{U}_{-+}\mathbf{U}_{--}\right)}_{\text{in } \mathcal{S}^l} \in \text{Span}\left\{\mathbf{U}^{-1}_{--}\mathbf{W} : \forall \mathbf{W} \in \mathcal{S}^l\right\}.\end{aligned} \tag{26}$$

The second part of the invariance property can be demonstrated in the same way. □

This result shows that the invariant space of $\mathbf{M}$ associated to the left-going modes can be described and approached by a part of the right non-reflection matrix $\widetilde{\mathbf{Z}}^{r,N_\beta}$ (or its limit $\widetilde{\mathbf{Z}}^r$). However, we have to apply once again a non-reflective boundary condition in the opposite direction in order to have access to all the eigenspaces generated by the eigenvectors of $\mathbf{M}$. It is necessary to do so to factorize entirely the propagation operator $\mathbf{M}$.

2.1.2. Approximation of the right invariant space

The developments of the previous section suggest using the left non-reflection matrix $\mathbf{Z}^{l,N_\beta}$, defined by:

$$\mathbf{Z}^{l,N_\beta} = \prod_{j=0}^{N_\beta-1}(\mathbf{M} - i\beta^j_+\mathbf{I})^{-1}(\mathbf{M} - i\beta^j_-\mathbf{I}), \tag{27}$$

in order to identify the right invariant space, i.e., the space of right-going modes associated to $\mathbf{M}$. This matrix is used in the Towne & Colonius left One-Way equations (resolution from right to left) and it allows to both "neutralize" the right-going modes and preserve the left-going ones.

From the matrix $\mathbf{Z}^{l,N_\beta}$, a "preconditioned" matrix $\widetilde{\mathbf{Z}}^{l,N_\beta}$ can be defined by:

$$\widetilde{\mathbf{Z}}^{l,N_\beta} = \begin{pmatrix} \mathbf{I}_{++} & \left(\mathbf{Z}^{l,N_\beta}_{++}\right)^{-1}\mathbf{Z}^{l,N_\beta}_{+-} \\ \left(\mathbf{Z}^{l,N_\beta}_{--}\right)^{-1}\mathbf{Z}^{l,N_\beta}_{-+} & \mathbf{I}_{--} \end{pmatrix}. \tag{28}$$

We then have the following result about the characterization of the right-going modes:

Theorem 2. *Let $(\beta^j_\pm)_{j\in\mathbb{N}}$ be a family of parameters adapted to the propagation operator $\mathbf{M}$ at the point x (see definition 1) whose a diagonalization is written $\mathbf{M} = \mathbf{VDU}$. We then have the two following results:*

i. The matrix subsequence $\widetilde{\mathbf{Z}}^{l,N_\beta}_{+-}$ admits a limit noted $\widetilde{\mathbf{Z}}^l_{-+}$ defined by:

$$\lim_{N_\beta\to+\infty}\widetilde{\mathbf{Z}}^{l,N_\beta}_{+-} = \widetilde{\mathbf{Z}}^l_{-+} = \mathbf{U}^{-1}_{++}\mathbf{U}_{+-}. \tag{29}$$

ii. We have the following identity:

$$\left(\widetilde{\mathbf{Z}}^l_{++} \quad \widetilde{\mathbf{Z}}^l_{+-}\right)\mathbf{M} = \left(\mathbf{U}^{-1}_{++}\mathbf{D}_{++}\mathbf{U}_{++}\right)\left(\widetilde{\mathbf{Z}}^l_{++} \quad \widetilde{\mathbf{Z}}^l_{+-}\right), \tag{30}$$

In addition, let $\mathcal{S}^r := S\,pan\left\{\mathbf{U}_{i,*} \in \mathbb{C}^{N_+ + N_-} | i = 1, ..., N_+\right\}$ be the right invariant space generated by the right eigenvectors of $\mathbf{M}$. Then the space

$$\widetilde{\mathcal{S}}^r := S\,pan\left\{\widetilde{\mathbf{Z}}^l_{i,*} \in \mathbb{C}^{N_+ + N_-} | i = 1, ..., N_+\right\} \tag{31}$$

verifies the right invariance property: $\forall\, \widetilde{\mathbf{W}} \in \widetilde{\mathcal{S}}^r$*, we have:*

$$\widetilde{\mathbf{W}}\mathbf{M} \ \in Span\left\{\mathbf{U}_{++}^{-1}\mathbf{W} :\ \forall\, \mathbf{W} \in \mathcal{S}^r\right\}, \tag{32}$$

and $\forall\, \mathbf{W} \in \mathcal{S}^r$*, we have:*

$$\mathbf{W}\mathbf{M} \ \in Span\left\{\mathbf{U}_{++}\widetilde{\mathbf{W}} :\ \forall\, \widetilde{\mathbf{W}} \in \widetilde{\mathcal{S}}^r\right\}. \tag{33}$$

Proof. The proof uses exactly the same arguments as the proof of theorem 1 in the context of left invariant space. □

This theorem shows that the invariant space associated to the eigenvalues α_+ can be characterized by the use of the matrix $\widetilde{\mathbf{Z}}^l$. This matrix comes from the non-reflecting boundary condition applied to the left. Thus, by using the matrices $\widetilde{\mathbf{Z}}^l$ and $\widetilde{\mathbf{Z}}^r$ at the same point x, it is possible to obtain a complete characterization of the invariant spaces of right and left-going modes. The combination of these two matrices will therefore allow the construction of a matrix of pseudo-eigenvectors, leading to a factorization of the matrix $\mathbf{M}$. The details of this operation are explained in the following section.

2.2. New factorization of the propagation operator and One-Way equations

From the theorems 1 and 2, we have the following results on the preconditioned non-reflection matrices:

$$\begin{aligned}
\lim_{N_\beta \to +\infty} \left(\mathbf{Z}_{--}^{r,N_\beta}\right)^{-1} \mathbf{Z}_{-+}^{r,N_\beta} &= \mathbf{U}_{--}^{-1}\mathbf{U}_{-+}, \\
\lim_{N_\beta \to +\infty} \left(\mathbf{Z}_{++}^{l,N_\beta}\right)^{-1} \mathbf{Z}_{+-}^{l,N_\beta} &= \mathbf{U}_{++}^{-1}\mathbf{U}_{+-},
\end{aligned} \tag{34}$$

where $\mathbf{U}$ is the exact eigenvectors' matrix resulting from the diagonalization of $\mathbf{M}$.

These results suggest introducing the following matrix $\widetilde{\mathbf{U}}^{N_\beta}$:

$$\widetilde{\mathbf{U}}^{N_\beta} := \begin{pmatrix} \mathbf{I}_{++} & \left(\mathbf{Z}_{++}^{l,N_\beta}\right)^{-1} \mathbf{Z}_{+-}^{l,N_\beta} \\ \left(\mathbf{Z}_{--}^{r,N_\beta}\right)^{-1} \mathbf{Z}_{-+}^{r,N_\beta} & \mathbf{I}_{--} \end{pmatrix}, \tag{35}$$

and by using $\widetilde{\mathbf{V}}^{N_\beta} = (\widetilde{\mathbf{U}}^{N_\beta})^{-1}$, we propose a new factorization of $\mathbf{M}$ as follows:

$$\widetilde{\mathbf{D}}^{N_\beta} := \widetilde{\mathbf{U}}^{N_\beta}\, \mathbf{M}\, \widetilde{\mathbf{V}}^{N_\beta}. \tag{36}$$

Finally, a direct application of the theorems 1 and 2 leads to the following fundamental decoupling result between left and right invariant spaces:

$$\lim_{N_\beta \to +\infty} \widetilde{\mathbf{D}}^{N_\beta} = \widetilde{\mathbf{D}} = \begin{pmatrix} \mathbf{U}_{++}^{-1}\, \mathbf{D}_{++}\mathbf{U}_{++} & \mathbf{0} \\ \mathbf{0} & \mathbf{U}_{--}^{-1}\, \mathbf{D}_{--}\mathbf{U}_{--} \end{pmatrix}, \tag{37}$$

where $\mathbf{D}_{++}$ and $\mathbf{D}_{--}$ are diagonal matrices containing the right- and left-going modes of $\mathbf{M}$, respectively.

This result implies that, by judiciously choosing a finite number N_β of parameters $\beta_\pm^j$ (cf. Fig. 6 in Section 4), we have:

$$\widetilde{\mathbf{D}}^{N_\beta} = \begin{pmatrix} \widetilde{\mathbf{D}}_{++}^{N_\beta} & \boldsymbol{\varepsilon}_{+-} \\ \boldsymbol{\varepsilon}_{-+} & \widetilde{\mathbf{D}}_{--}^{N_\beta} \end{pmatrix}, \tag{38}$$

where $\widetilde{\mathbf{D}}_{++}^{N_\beta}$ and $\widetilde{\mathbf{D}}_{--}^{N_\beta}$ are two block matrices containing information about the eigenvalues of $\mathbf{M}$ and $\boldsymbol{\varepsilon}_{+-}$ and $\boldsymbol{\varepsilon}_{-+}$ are two negligible block matrices containing the residues of the approximation and which tend to $\mathbf{0}$ when $N_\beta \to +\infty$.

Finally, the approximate factorization of the propagation operator $\mathbf{M}$ is written as:

$$\widetilde{\mathbf{M}} = \widetilde{\mathbf{V}}^{N_\beta} \widetilde{\widetilde{\mathbf{D}}}^{N_\beta} \widetilde{\mathbf{U}}^{N_\beta} \approx \mathbf{M}, \tag{39}$$

with

$$\widetilde{\widetilde{\mathbf{D}}}^{N_\beta} = \begin{pmatrix} \widetilde{\mathbf{D}}_{++}^{N_\beta} & \mathbf{0} \\ \mathbf{0} & \widetilde{\mathbf{D}}_{--}^{N_\beta} \end{pmatrix}. \tag{40}$$

The extra-diagonal residual terms are neglected, allowing a complete decoupling of right and left-going modes.

Remark 1. *Unlike a direct spectral decomposition, the numerical factorization* (39) *and* (40) *of the propagation operator allows to naturally sort the modes according to their direction of propagation.*

Thanks to the approximate factorization (39) of $\mathbf{M}$, we can directly derive One-Way equations in One-Way variables. In this way, we also have access to accurate information about the refraction and transmission phenomena, which occur in function of the complexity of the mean flow. More precisely, we can construct One-Way equations (True amplitude version or Bremmer series) which have a wider domain of validity [20] than classical formulations such as those proposed by Towne & Colonius. Furthermore, the accuracy of this information will be used in the next section to construct precise transmission conditions in the presence of discontinuities in the domain.

Now, by performing the variable change $\boldsymbol{\phi} = \widetilde{\mathbf{V}}^{N_\beta} \boldsymbol{\psi}$, Eq. (5) can be written in One-Way variables:

$$\frac{\mathrm{d}}{\mathrm{d}x} \begin{pmatrix} \boldsymbol{\psi}_+ \\ \boldsymbol{\psi}_- \end{pmatrix} = \begin{pmatrix} \widetilde{\mathbf{D}}_{++}^{N_\beta} & \mathbf{0} \\ \mathbf{0} & \widetilde{\mathbf{D}}_{--}^{N_\beta} \end{pmatrix} \begin{pmatrix} \boldsymbol{\psi}_+ \\ \boldsymbol{\psi}_- \end{pmatrix} + \begin{pmatrix} \widetilde{\mathbf{W}}_{++}^{N_\beta} & \widetilde{\mathbf{W}}_{+-}^{N_\beta} \\ \widetilde{\mathbf{W}}_{-+}^{N_\beta} & \widetilde{\mathbf{W}}_{--}^{N_\beta} \end{pmatrix} \begin{pmatrix} \boldsymbol{\psi}_+ \\ \boldsymbol{\psi}_- \end{pmatrix}, \tag{41}$$

where the matrix $\widetilde{W}^{N_\beta} := -\widetilde{\mathbf{U}}^{N_\beta} \dfrac{\mathrm{d}\widetilde{\mathbf{V}}^{N_\beta}}{\mathrm{d}x}$ is called the refraction/refraction operator.

The first step in constructing the One-Way equations is the decoupling between the variables $\boldsymbol{\psi}_+$ and $\boldsymbol{\psi}_-$ i.e., the left and right-going information. For this, the extra-diagonal terms in the matrix $\widetilde{W}^{N_\beta}$ are neglected, i.e., $\widetilde{\mathbf{W}}_{+-}^{N_\beta} = \widetilde{\mathbf{W}}_{-+}^{N_\beta} = \mathbf{0}$ and Eq. (41) leads to:

$$\frac{\mathrm{d}}{\mathrm{d}x} \begin{pmatrix} \boldsymbol{\psi}_+ \\ \boldsymbol{\psi}_- \end{pmatrix} = \begin{pmatrix} \widetilde{\mathbf{D}}_{++}^{N_\beta} + \widetilde{\mathbf{W}}_{++}^{N_\beta} & \mathbf{0} \\ \mathbf{0} & \widetilde{\mathbf{D}}_{--}^{N_\beta} + \widetilde{\mathbf{W}}_{--}^{N_\beta} \end{pmatrix} \begin{pmatrix} \boldsymbol{\psi}_+ \\ \boldsymbol{\psi}_- \end{pmatrix}. \tag{42}$$

Neglecting these terms is mandatory to resolve a well-posed system, but it is also at the origin of the so-called slowly varying flow hypothesis [15] along the privileged direction (x in our case). From Equation (42), two types of One-Way equations can be derived:

1/ The right and left standard One-Way equations obtained by neglecting the terms $\widetilde{\mathbf{W}}_{++}^{N_\beta}$ and $\widetilde{\mathbf{W}}_{--}^{N_\beta}$:

$$\begin{cases} \dfrac{\mathrm{d}\boldsymbol{\psi}_+}{\mathrm{d}x} = \widetilde{\mathbf{D}}_{++}^{N_\beta} \boldsymbol{\psi}_+, \\ \boldsymbol{\psi}_- = \mathbf{0}, \end{cases} \text{(Right One-Way)} \tag{43}$$

and

$$\begin{cases} \dfrac{\mathrm{d}\boldsymbol{\psi}_-}{\mathrm{d}x} = \widetilde{\mathbf{D}}_{--}^{N_\beta}\boldsymbol{\psi}_-, \\ \boldsymbol{\psi}_+ = \mathbf{0}, \end{cases} \quad \text{(Left One-Way)} \tag{44}$$

These equations accurately reproduce the spatial frequencies of the signal, but the amplitude may be inaccurate when the two terms $\widetilde{\mathbf{W}}_{++}^{N_\beta}$ and $\widetilde{\mathbf{W}}_{--}^{N_\beta}$ are not negligible enough.

2/ The right and left True Amplitude One-Way equations:

$$\begin{cases} \dfrac{\mathrm{d}\boldsymbol{\psi}_+}{\mathrm{d}x} = \left(\widetilde{\mathbf{D}}_{++}^{N_\beta} + \widetilde{\mathbf{W}}_{++}^{N_\beta}\right)\boldsymbol{\psi}_+, \\ \boldsymbol{\psi}_- = \mathbf{0}, \end{cases} \quad \text{(Right True Amplitude One-Way)} \tag{45}$$

and

$$\begin{cases} \dfrac{\mathrm{d}\boldsymbol{\psi}_-}{\mathrm{d}x} = \left(\widetilde{\mathbf{D}}_{--}^{N_\beta} + \widetilde{\mathbf{W}}_{--}^{N_\beta}\right)\boldsymbol{\psi}_-, \\ \boldsymbol{\psi}_+ = \mathbf{0}, \end{cases} \quad \text{(Left True Amplitude One-Way)} \tag{46}$$

These equations accurately reproduce both the spatial frequencies and the amplitude of the signal.

Remark 2. *Towne & Colonius One-Way formulation belongs to the first category.*

Remark 3. *The case where the baseflow is parallel throughout the computational domain leads to a matrix $\widetilde{\mathbf{V}}^{N_\beta}$ independent of the x variable, which means that neglecting the $\widetilde{W}^{N_\beta}$ term does not generate an approximation of the model.*

Finally, the numerical integration of the equations (43), (44), (45) and (46) is realized from a Discontinuous Galerkin scheme adapted to the first-order hyperbolic equation [24]. This approach leads to an unconditionally stable explicit resolution [20].

To simplify the notations, the factorization (39) will now be defined by $\mathbf{M} = \widetilde{\mathbf{V}}\widetilde{\mathbf{D}}\widetilde{\mathbf{U}}$ in the rest of this paper.

3. Domain decomposition method for lined ducts

3.1. Principle

The fact that the right and left-going One-Way equations are being solved through a spatial marching algorithm means that when a discontinuity is encountered (in our case the leading and trailing edges of the acoustic liner section), a particular treatment has to be applied in order to get a relevant solution. As a matter of fact, the variables used for the resolution (i.e., $\boldsymbol{\psi}$-variables) are projected into a given space of application that depends on the baseflow and the boundary conditions applied on the top and the bottom of the duct. When these boundary conditions are modified through a discontinuity, if no special treatment is applied to the One-Way variables, their projection back into the physical space (i.e., in primitive variables), will create a discrepancy in the result obtained since the transformation matrices $\widetilde{\mathbf{U}}$ and $\widetilde{\mathbf{V}}$ are not equivalent on each side of the discontinuity. Moreover, the incident wave propagating across such a discontinuity will be split into a transmitted wave, that will propagate in the same direction but with a modified wavelength and amplitude, and into a reflected wave, propagating in the opposite direction.

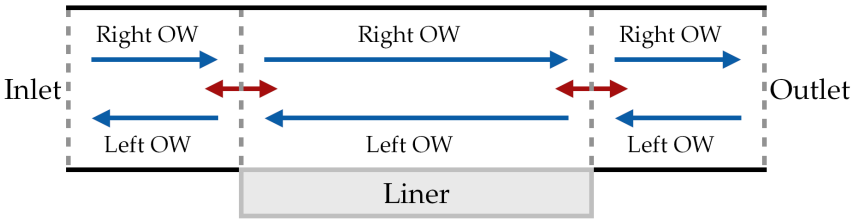

Figure 1: Decomposition of the computational domain.

The model setting considered in the paper is a 2D rectangular duct with an acoustic liner on the down wall as described in Fig. 1. The baseflow is assumed to be smooth in the whole computational domain and consequently, the resolution by One-Way equations is valid everywhere except directly on top of the discontinuities of boundary conditions (represented by the internal dashed lines in Fig. 1). Therefore, the domain of computation is naturally split in three non-overlapping subdomains where standard One-Way equations are solved while the computation of the reflected and transmitted waves will occur only at their interfaces. Because both left- and right-going waves will exist in each subdomain, both a right-going One-Way equation (called right One-Way) and a left-going One-Way equation (called left One-Way) have to be solved in order to take into account the reflected and transmitted waves created by these discontinuities.

We propose an iterative domain decomposition method to compute an accurate approximation of the complete solution. We will now describe the sketch of this algorithm. For that, we introduce some notations: $(\Omega_i)_{i=1}^3$ are the subdomains from left to right, Γ^{in} is the inlet interface, $\Gamma_{12} = \Omega_1 \cap \Omega_2$, $\Gamma_{23} = \Omega_2 \cap \Omega_3$ and Γ^{out} is the outlet interface, $\boldsymbol{\psi}_{\pm}^{i,n}$ is the solution in Ω_i at the iteration n. In addition, incoming and outgoing sources are prescribed at the inlet Γ^{in} and outlet Γ^{out} boundaries, i.e., $\boldsymbol{\psi}_{+|\Gamma^{in}} = \boldsymbol{g}^{in}$ and $\boldsymbol{\psi}_{-|\Gamma^{out}} = \boldsymbol{g}^{out}$. By taking the initial guess $\psi_{\pm}^{i,0} = \mathbf{0}$ and formally introducing the left and right transmission operators $T_{k\to l}$ and $T_{k\leftarrow l}$ associated with the Γ_{kl} interface, the computation on each subdomain is performed as follows:

- In the inlet subdomain Ω_1:
  - $\boldsymbol{\psi}_{+}^{1,n+1} = \boldsymbol{\psi}_{+}^{1,1}$ is obtained in only one iteration due to the decoupling property of this variable:
$$\begin{cases} \dfrac{\mathrm{d}\boldsymbol{\psi}_{+}^{1,1}}{\mathrm{d}x} = \widetilde{\mathbf{D}}_{++}\boldsymbol{\psi}_{+}^{1,1} \text{ in } \Omega_1, \\ \boldsymbol{\psi}_{+}^{1,1} = \boldsymbol{g}^{in} \text{ on } \Gamma^{in}. \end{cases} \tag{47}$$
  - $\boldsymbol{\psi}_{-}^{1,n+1}$ is computed as follows:
$$\begin{cases} \dfrac{\mathrm{d}\boldsymbol{\psi}_{-}^{1,n+1}}{\mathrm{d}x} = \widetilde{\mathbf{D}}_{--}\boldsymbol{\psi}_{-}^{1,n+1} \text{ in } \Omega_1, \\ \boldsymbol{\psi}_{-}^{1,n+1} = \mathrm{T}_{1\leftarrow 2}\left(\boldsymbol{\psi}_{\pm}^{1,n}, \boldsymbol{\psi}_{\pm}^{2,n}\right) \text{ on } \Gamma_{12}. \end{cases} \tag{48}$$
- In the liner subdomain Ω_2:

- $\boldsymbol{\psi}_{+}^{2,n+1}$ is computed as follows:

$$\begin{cases} \dfrac{\mathrm{d}\boldsymbol{\psi}_{+}^{2,n+1}}{\mathrm{d}x} = \widetilde{\mathbf{D}}_{++}\boldsymbol{\psi}_{+}^{2,n+1} \text{ in } \Omega_2, \\ \boldsymbol{\psi}_{+}^{2,n+1} = \mathrm{T}_{1\to 2}\left(\boldsymbol{\psi}_{\pm}^{1,n}, \boldsymbol{\psi}_{\pm}^{2,n}\right) \text{ on } \Gamma_{12}. \end{cases} \tag{49}$$

- $\boldsymbol{\psi}_{-}^{2,n+1}$ is computed as follows:

$$\begin{cases} \dfrac{\mathrm{d}\boldsymbol{\psi}_{-}^{2,n+1}}{\mathrm{d}x} = \widetilde{\mathbf{D}}_{--}\boldsymbol{\psi}_{-}^{2,n+1} \text{ in } \Omega_2, \\ \boldsymbol{\psi}_{-}^{2,n+1} = \mathrm{T}_{2\leftarrow 3}\left(\boldsymbol{\psi}_{\pm}^{2,n}, \boldsymbol{\psi}_{\pm}^{3,n}\right) \text{ on } \Gamma_{23}. \end{cases} \tag{50}$$

- In the outlet subdomain Ω_3:

  - $\boldsymbol{\psi}_{+}^{3,n+1}$ is computed as follows:

$$\begin{cases} \dfrac{\mathrm{d}\boldsymbol{\psi}_{+}^{3,n+1}}{\mathrm{d}x} = \widetilde{\mathbf{D}}_{++}\boldsymbol{\psi}_{+}^{3,n+1} \text{ in } \Omega_3, \\ \boldsymbol{\psi}_{+}^{3,n+1} = \mathrm{T}_{2\to 3}\left(\boldsymbol{\psi}_{\pm}^{2,n}, \boldsymbol{\psi}_{\pm}^{3,n}\right) \text{ on } \Gamma_{23}. \end{cases} \tag{51}$$

  - $\boldsymbol{\psi}_{-}^{3,n+1} = \boldsymbol{\psi}_{-}^{3,1}$ is obtained in only one iteration due to the decoupling property of this variable:

$$\begin{cases} \dfrac{\mathrm{d}\boldsymbol{\psi}_{-}^{3,1}}{\mathrm{d}x} = \widetilde{\mathbf{D}}_{--}\boldsymbol{\psi}_{-}^{3,1} \text{ in } \Omega_3, \\ \boldsymbol{\psi}_{-}^{3,1} = \boldsymbol{g}^{out} \text{ on } \Gamma^{out}. \end{cases} \tag{52}$$

Remark 4. *In each subdomain, left and right One-Way resolutions are performed to capture the left- and right-going waves propagating into each subdomain, the reflection, and refraction of these waves have to be computed at each interface. These computed waves will then be used in the next iteration to initialize another computation of left and right One-Way equations. At each iteration, the obtained result will become more and more accurate, as reflections and transmissions of the previous approximation are included. These iterations can be carried out until the convergence is considered satisfactory.*

Remark 5. *In the description of the domain decomposition algorithm, the True Amplitude version of One-Way equations can obviously be used for local resolution if the refraction/refraction matrix is not negligible.*

In the next subsection, we propose efficient candidates for the transmission boundary conditions $T_{k\to l}$ and $T_{k\leftarrow l}$ associated to the discontinuity interface Γ_{kl} by exploiting the projection operators induced by the numerical factorization of the propagation operator presented previously in Section 2.

3.2. Transmission conditions

In the following, we will focus on the specific example of the interface Γ_{12} and then we will have a result that will enable us to process the interface Γ_{kl} using the transmission operators

$T_{k\to l}$ and $T_{k\leftarrow l}$. At each interface, the incident waves (coming from the left and right subdomains) have to be sorted in order to communicate properly the waves exiting the current domain, entering it or reflected inside. To do that, the information contained inside the newly formed pseudo-eigenvectors matrices $\widetilde{\mathbf{U}}$ and $\widetilde{\mathbf{V}}$ will be used to project the One-Way variables of a domain back into their primitive form before projecting them into the One-Way variables of the next subdomain. The idea is that we want the physical variables to be continuous even across the discontinuity, therefore, the objective is to impose the following relation at the interface Γ_{12}:

$$\widetilde{\mathbf{q}}^1 = \widetilde{\mathbf{q}}^2, \tag{53}$$

with $\widetilde{\mathbf{q}}^1$ the discretized perturbation vector situated at the interface but from the left domain and $\widetilde{\mathbf{q}}^2$ the same discretized perturbation vector at the interface but from the right domain. For the rest of this development, these subscripts have the same meaning when applied to other variables or matrices. In addition, the derivation of this domain decomposition is done, here, for the first discontinuity i.e., a hard wall boundary condition on the left and an impedance condition on the right), but the same development can be done for the second discontinuity located at the liner's trailing edge. Generally, this condition alone can present some convergence issues and is usually associated with, for example, a condition of continuity on the variable's gradient across the interface [25]. However, in our case, because the condition (53) can be expressed in terms of One-Way variables that are already decomposed in left- and right-going components, this additional condition is not necessary. To express Equation (53) in terms of One-Way variables $\boldsymbol{\psi}^1$ and $\boldsymbol{\psi}^2$, it is first required to use the characteristic variables:

$$\mathbf{T}^1\boldsymbol{\phi}^1 = \mathbf{T}^2\boldsymbol{\phi}^2. \tag{54}$$

Here, this condition can be simplified since the two different boundary conditions involved do not affect the expression of the transformation matrix $\mathbf{T}$. Therefore, Eq. (54) becomes:

$$\boldsymbol{\phi}^1 = \boldsymbol{\phi}^2. \tag{55}$$

By applying the second variable change with the pseudo eigenvectors matrices $\widetilde{\mathbf{V}}$, the continuity condition takes the following form in terms of One-Way variables:

$$\widetilde{\mathbf{V}}^1\boldsymbol{\psi}^1 = \widetilde{\mathbf{V}}^2\boldsymbol{\psi}^2. \tag{56}$$

In the same way as before, the matrix $\widetilde{\mathbf{V}}$ can be separated into its + and − components such as:

$$\begin{cases} \widetilde{\mathbf{V}}^1_{++}\boldsymbol{\psi}^1_+ + \widetilde{\mathbf{V}}^1_{+-}\boldsymbol{\psi}^1_- = \widetilde{\mathbf{V}}^2_{++}\boldsymbol{\psi}^2_+ + \widetilde{\mathbf{V}}^2_{+-}\boldsymbol{\psi}^2_-, \\ \widetilde{\mathbf{V}}^1_{-+}\boldsymbol{\psi}^1_+ + \widetilde{\mathbf{V}}^1_{--}\boldsymbol{\psi}^1_- = \widetilde{\mathbf{V}}^2_{-+}\boldsymbol{\psi}^2_+ + \widetilde{\mathbf{V}}^2_{--}\boldsymbol{\psi}^2_-. \end{cases} \tag{57}$$

This expression of the continuity relation (53) gives the separation in left- and right-going components of the waves at the interface. The next step is to determine which part of the incoming wave is sent back into the original domain and which part is transmitted to the next one. The setup in which the domain decomposition is performed is shown in Figure 2. The previous iteration of left and right One-Way resolutions gives an approximation of the incident waves that takes the form of $\boldsymbol{\psi}^+_1$ from the inlet subdomain and $\boldsymbol{\psi}^2_-$ from the liner subdomain. Therefore, these two variables now become a known element in Equation (57). This transmission problem then becomes a system of two equations with two variables that can easily be solved. This equation

gives an approximation of the outgoing waves that depend on the degree of precision of the given information (in this case, $\boldsymbol{\psi}_+^1$ and $\boldsymbol{\psi}_-^2$) that improves depending on the number of iterations.

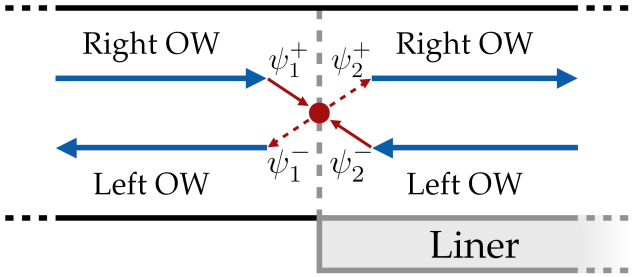

Figure 2: Transmission of wave through a discontinuity.

The missing values $\boldsymbol{\psi}_+^2$ and $\boldsymbol{\psi}_-^1$ can easily be expressed from $\boldsymbol{\psi}_+^1$ and $\boldsymbol{\psi}_-^2$ under the following form:

$$\begin{cases} \boldsymbol{\psi}_+^2 = (\widetilde{\mathbf{V}}_{++}^2 - \widetilde{\mathbf{V}}_{+-}^1(\widetilde{\mathbf{V}}_{--}^1)^{-1}\widetilde{\mathbf{V}}_{-+}^2)^{-1}((\widetilde{\mathbf{V}}_{++}^1 - \widetilde{\mathbf{V}}_{+-}^1(\widetilde{\mathbf{V}}_{--}^1)^{-1}\widetilde{\mathbf{V}}_{-+}^1)\boldsymbol{\psi}_+^1 \\ \qquad - (\widetilde{\mathbf{V}}_{+-}^2 - \widetilde{\mathbf{V}}_{+-}^1(\widetilde{\mathbf{V}}_{--}^1)^{-1}\widetilde{\mathbf{V}}_{--}^2)\boldsymbol{\psi}_-^2), \\ \boldsymbol{\psi}_-^1 = (\widetilde{\mathbf{V}}_{--}^1)^{-1}(\widetilde{\mathbf{V}}_{-+}^2\boldsymbol{\psi}_+^2 + \widetilde{\mathbf{V}}_{--}^2\boldsymbol{\psi}_-^2 - \widetilde{\mathbf{V}}_{-+}^1\boldsymbol{\psi}_+^1). \end{cases} \tag{58}$$

The newly obtained values can then be set as initialization for the left One-Way resolution in the inlet subdomain and for the right One-Way resolution in the liner subdomain.

The relations (58) can now be generalized and lead to the following proposition for the transmission operators $T_{k\to l}$ and $T_{k\leftarrow l}$:

$$\begin{cases} \mathrm{T}_{k\to l}(\boldsymbol{\psi}_\pm^{k,n}, \boldsymbol{\psi}_\pm^{l,n}) = C_{k\to l}\ ((\widetilde{\mathbf{V}}_{++}^k - \widetilde{\mathbf{V}}_{+-}^k(\widetilde{\mathbf{V}}_{--}^k)^{-1}\widetilde{\mathbf{V}}_{-+}^k)\boldsymbol{\psi}_+^{k,n} \\ \qquad\qquad - (\widetilde{\mathbf{V}}_{+-}^l - \widetilde{\mathbf{V}}_{+-}^k(\widetilde{\mathbf{V}}_{--}^k)^{-1}\widetilde{\mathbf{V}}_{--}^l)\boldsymbol{\psi}_-^{l,n}), \\ \mathrm{T}_{k\leftarrow l}(\boldsymbol{\psi}_\pm^{k,n}, \boldsymbol{\psi}_\pm^{l,n}) = C_{k\leftarrow l}\ (\widetilde{\mathbf{V}}_{-+}^l\boldsymbol{\psi}_+^{l,n} + \widetilde{\mathbf{V}}_{--}^l\boldsymbol{\psi}_-^{l,n} - \widetilde{\mathbf{V}}_{-+}^k\boldsymbol{\psi}_+^{k,n}), \end{cases} \tag{59}$$

with $C_{k\to l} := (\widetilde{\mathbf{V}}_{++}^l - \widetilde{\mathbf{V}}_{+-}^k(\widetilde{\mathbf{V}}_{--}^k)^{-1}\widetilde{\mathbf{V}}_{-+}^l)^{-1}$ and $C_{k\leftarrow l} := (\widetilde{\mathbf{V}}_{--}^k)^{-1}$.

4. Numerical applications

4.1. Governing equations

To simulate the propagation of waves inside this partially lined duct, the linearized Euler and Navier-Stokes equations presented in this section are the base of the One-Way equations (see Section 2) that will effectively be solved.

The linearized Euler and Navier-Stokes equations neglect the effects of the non-linear phenomena that could appear inside the flow but, since the range of frequencies and Sound Pressure Level (SPL) we consider predominantly involve linear mechanisms, this approximation is well adapted and gives accurate results [26, 27]. To linearize the Euler and Navier-Stokes equations, the following classical decomposition is used:

$$q(x, y, t) = \overline{q}(x, y) + q'(x, y, t), \tag{60}$$

where $\overline{q}$ is the variable of the steady baseflow around which the equations are linearized and q' represents the perturbations' vector. For Euler equations, we will consider $q = (p, u, v)^T$ and for Navier-Stokes equations, we will consider $q = (v, u, v, p)^T$, with $v = 1/\rho$ the specific volume, $\mathbf{u} = (u, v)^T$ the velocity vector and p the pressure. In the following, we will also assume that $\overline{u} = \overline{u}(y)$ (its expression is given below for two cases), $\overline{v} = 0$, $\overline{\rho} = \rho_0$ a constant and $\overline{p} = p_0$ a constant.

In both cases, we can then rewrite the system of equations under the following form:

$$\frac{\partial q'}{\partial t} + A\frac{\partial q'}{\partial x} + B_y\frac{\partial q'}{\partial y} + B_{xx}\frac{\partial^2 q'}{\partial x^2} + B_{xy}\frac{\partial^2 q'}{\partial x \partial y} + B_{yy}\frac{\partial^2 q'}{\partial y^2} + Cq' = 0 \tag{61}$$

To obtain a system of linear hyperbolic equations of type (1), second derivatives in x and cross derivatives in Navier-Stokes equations are neglected, as it is generally the case in One-Way approaches [28, 29]. We next proceed as explained in Section 2 by choosing the privileged direction x, consider the equations in the harmonic regime and then discretize them in the transverse direction y.

The different operator matrices are given in Appendix A, for both linearized Euler and Navier-Stokes equations and by taking into account the characteristics of the baseflow.

4.2. Partially lined duct

4.2.1. Configuration of the lined duct

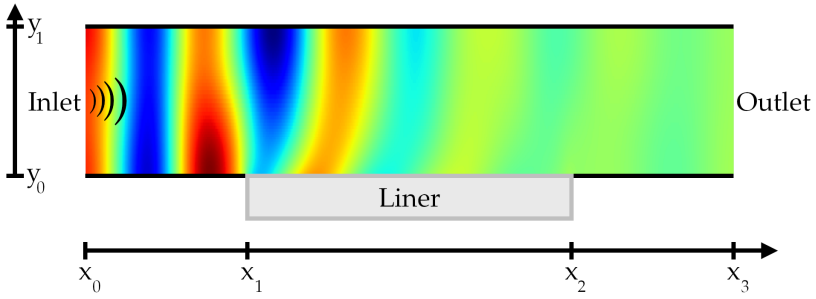

Figure 3: Configuration of the lined duct.

The partially lined duct configuration is presented in this section, along with the different baseflows used for the comparison with experimental data and with several numerical simulations. The experimental configuration on which these simulations are based is taken from [30]. The data provided by this study have been widely used for the validation of codes in 2-D and 3-D with a resolution in time or frequency domain [31, 32]. Therefore, the duct presents a partially lined section on the bottom (the experimental facility has it on the top) with a length $L_{liner} = x_2 - x_1 = 0.406$ m with $x_1 = 0.203$ m and $x_2 = 0.609$ m. The full duct has a total length of $L_x = x_3 - x_0 = 0.812$ m with $x_0 = 0$ and $x_3 = 0.812$ m. The height of this section is $L_y = y_1 - y_0 = 0.051$ m with $y_0 = 0$ and $y_1 = 0.051$ m. The configuration of the duct is represented in Figure 3 with an example of the real part of the pressure computed for a 3000 Hz case with a Poiseuille flow. In the different 2-D simulations performed in this paper, a fully right-propagating plane wave is imposed at the inlet. Its expression has been obtained through a local

modal analysis of the baseflow at $x = x_0$. On the other hand, no left-going wave is imposed at the outlet, meaning that any wave reflected after x_3 is neglected.

Concerning the baseflow, two cases are studied here. In both cases, the baseflow represents a fully developed laminar or turbulent Poiseuille flow with different boundary layer thicknesses and different values of the maximum Mach number M_{max} but with the same mean Mach number $M_{mean} = 0.335$, which is the value used in the experimental setup [30]. Moreover, only the axial velocity is imposed, and the same profile is used everywhere inside the computational domain. Case 1 presents a parallel laminar flow modeled by the following equation [2]:

$$\overline{u}(y) = 4M_{max}a\frac{y}{L_y}\left(1 - \frac{y}{L_y}\right), \tag{62}$$

where $M_{max} = 0.5025$ is the maximum Mach number and a is the speed of sound. The value has been chosen to ensure a mean Mach number of 0.335.

On the other hand, in Case 2, the parallel turbulent flow is approached by the following equation:

$$\overline{u}(y) = Ma\frac{n_y + 1}{n_y}\left(1 - \left|1 - \frac{2y}{L_y}\right|^{n_y}\right), \tag{63}$$

where n_y is the coefficient parameterizing the boundary layer thickness and $M = 0.335$. The value of this coefficient will differ depending on whether a OWNS or OWE simulation is performed. This expression is taken from [33] where the third component along the z-axis has been removed, since the One-Way simulations are performed in 2-D. This expression of the Poiseuille flow presents a thinner boundary layer than the one taken in [33]. In Figure 4, the baseflow profiles are plotted along the transverse direction with the experimental data taken in the center of the duct.

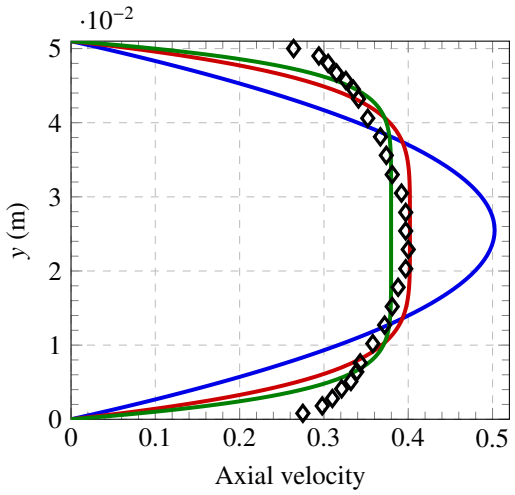

Figure 4: Dimensionless axial velocity of the baseflow used for the Case 1 (——) and the Case 2 with $n_y = 5$ (——) and $n_y = 7.5$ (——) compared with experimental data (◇) from [30].

4.2.2. Transverse boundary conditions

Hard wall. The hard wall boundary conditions are applied at the top of the duct and on each side of the acoustic liner. This condition is modeled differently for Euler and Navier-Stokes

equations. In the case of Euler equations, the hard wall is modeled by a slip boundary condition which allows the particles to slip tangentially to the wall while imposing the normal velocity v to 0 in order to satisfy the continuity of mass. Moreover, this slip boundary condition is equivalent to modelling an infinitely thin acoustic boundary layer [34, 2] and it satisfies the following set of equations:

$$\begin{cases} -i\omega\widetilde{p} + \overline{u}\dfrac{\partial\widetilde{p}}{\partial x} + \overline{\rho}a^2\left(\dfrac{\partial\widetilde{u}}{\partial x} + \dfrac{\partial\widetilde{v}}{\partial y}\right) + S\,a\dfrac{\partial\widetilde{p}}{\partial y} = 0, \\ -i\omega\widetilde{u} + \overline{u}\dfrac{\partial\widetilde{u}}{\partial x} + \dfrac{1}{\overline{\rho}}\dfrac{\partial\widetilde{p}}{\partial x} = 0, \\ -i\omega\widetilde{v} + \overline{u}\dfrac{\partial\widetilde{v}}{\partial x} = 0, \end{cases} \tag{64}$$

with $S = 1$ or $S = -1$ for the upper or lower wall, respectively. Since the One-Way equations can also be solved in terms of characteristic variables, the expression of this boundary condition is given in Appendix B.

In the case of Navier-Stokes equations, we need to impose an isothermal no-slip boundary condition, which can be written as:

$$\widetilde{u} = \widetilde{v} = \widetilde{T} = 0. \tag{65}$$

where the temperature perturbation $\widetilde{T}$ is obtained by linearizing the equation of state.

Acoustic liner. The impedance condition is applied following the classical relation:

$$\widetilde{p} = Z(\omega)\widetilde{\mathbf{u}}\cdot\mathbf{n}, \tag{66}$$

with $\mathbf{n}$ the unitary outward pointing normal to the wall and $Z(\omega)$ the frequency dependent complex impedance, which means, in our case, that its value has to be modified according to the value of ω set. The impedance model is taken from [33] and was used, originally, to model the behavior of Z for high frequency values (> 3000 Hz), but is in good accordance with the experimental data that are available up to 3000 Hz. The expression of this impedance is given by:

$$Z(\omega) = \frac{1}{\sigma}\coth(-ik_c(\omega)l_c), \tag{67}$$

with σ the porosity of the liner's surface, k_c the acoustic wave number inside the liner's tube and l_c the tube length. All the expressions needed for the construction of this model are available in [33] along with the values of the coefficients depending on the type of liner used (CT57 in our case) and the mean velocity of the baseflow. In Figure 5, the real and imaginary parts of $Z(\omega)$ are plotted for a mean Mach number of 0.335. The values are also compared to experimental impedance data from [30]. It can be noted that, in our case, the expression of the impedance corresponds to $e^{-i\omega t}$ convention. For the usual acoustic convention $e^{i\omega t}$, the conjugate value of $Z(\omega)$ should be taken.

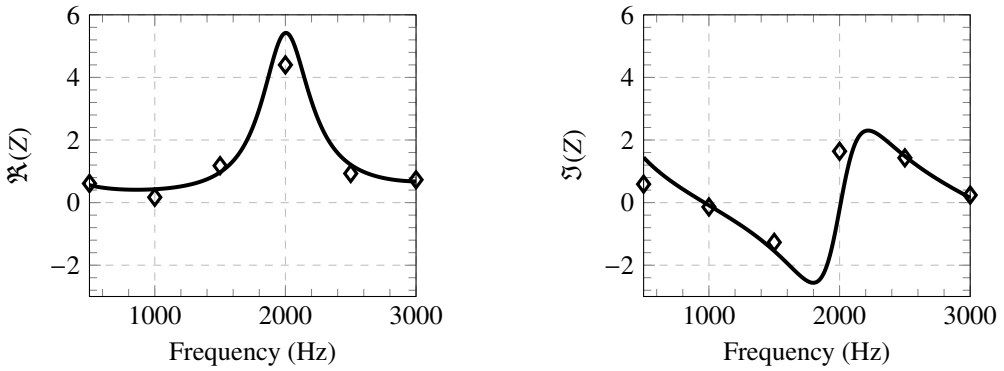

(a) Real part of the impedance

(b) Imaginary part of the impedance

Figure 5: Real and imaginary parts of the impedance Z of the CT57 liner for $M_{mean} = 0.335$: experimental data (◇) and numerical values (——) obtained by using the model from [33].

Remark 6. *The boundary conditions being implemented in practice in characteristic variables $\boldsymbol{\phi}$, their expressions can be found in Appendix B.*

4.3. Numerical results

The numerical results presented here have been computed on both different configurations presented above. To compare the results obtained with OWE and OWNS simulations with experimental data and other numerical results, the sound pressure level (SPL) is defined as follows:

$$\text{SPL} = 20 \log\left(\frac{|\widetilde{p}|}{p_{\text{ref}}}\right), \tag{68}$$

with $p_{\text{ref}} = 2 \times 10^{-5}$ Pa the reference sound pressure. The SPL is expressed in decibels (dB).

In both cases, the One-Way simulations have been initialized by a 130 dB harmonic plane wave mode obtained by the resolution of a modal stability analysis at the inlet of the computational domain (left source). These plane waves have been scaled to get a similar SPL as in the numerical experiments.

The propagation of the waves inside the partially lined duct is computed with the two different baseflows presented in Section 4.2.1. The presence of an unstable mode at 1000 Hz has already been reported in several studies [31, 32, 35, 36, 33], due to the presence of a surface mode when the flow profile is highly sheared at the wall.

The different simulations have been carried out with a 4^{th} to 6^{th} order finite difference compact scheme [22] in the transverse direction, while the resolution along the x-axis is done by a second-order upwind Discontinuous Galerkin method [24]. Concerning the number of discretization points, most of the cases have been simulated with 173 points (133 points were sufficient for the 2000 Hz case) in the transverse direction, with a mesh constructed from local refinement near the duct walls in order to accurately take into account very thin Stokes layers' phenomenon occurring in Navier-Stokes simulations and to correctly capture the propagating waves. In addition, 1000 points were required in x for the marching algorithm.

The required number of $\beta_{\pm}$ coefficients is 15 for all the simulations (OWE and OWNS). A comparison between the approximate spectrum resulting from factorization and the exact spectrum at $f = 2000$ Hz in Case 1 with a OWE simulation is represented in Figure 6. We can see

that the two spectra match very well, for a limited number of parameters. The convergence of the numerical One-Way method is ensured by placing these parameters "close" to the spectrum of the propagation operator $\mathbf{M}$, i.e., β_+ close to the positive eigenvalues and β_- close to the negative eigenvalues. In practice, we are using some information on the exact operator spectrum such as the branch position of evanescent modes or the range of convective modes branch, which are deduced from a local modal analysis. The choice of placement of $\beta_\pm$ coefficients and the influence of their number on the method convergence are discussed at greater length in [20].

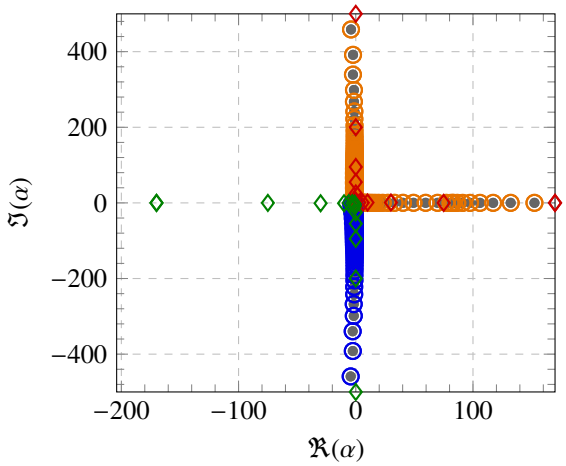

Figure 6: Comparison between the approximate modes from factorization with the exact modes for 15 β_+ (◇) and 15 β_- (◇) coefficients and for a OWE simulation at 2000 Hz: α (●) corresponds to the exact operator spectrum, λ_+ (○) to the spectrum of $\widetilde{\mathbf{D}}_{++}$ and λ_- (○) to the spectrum of $\widetilde{\mathbf{D}}_{--}$.

4.3.1. Comparison between the two baseflows and the OWE and OWNS simulations

The SPL values on the wall opposed to the acoustic liner are plotted in Figure 7 together with the experimental data [30] and a numerical result from [33] (for the 1000, 2000 and 3000 Hz frequencies) that has been obtained through a mode-matching method based on the linearized Euler equations. This last numerical result is obtained for a baseflow that is slightly different to the one used here for the One-Way simulations. As a matter of fact, the coefficient used to parameter the boundary layer thickness is $n_y = 24$ as opposed to a value of 5 and 7.5 (for the OWE and OWNS simulations, respectively).

Our first approach was to consider a laminar Poiseuille baseflow profile (Case 1) for both OWE and OWNS simulations. In all six cases, the One-Way simulations are noticeably close to each other, and the results are also pretty similar to the mode-matching method [33] for all the frequencies investigated here. In the same way, the One-Way results match closely the experimental data except for the 1000 and 3000 Hz cases where a difference of around 10 dB can be seen. This discrepancy in accuracy can be explained by several factors. Firstly, this lined duct configuration presents a resonance frequency around 1000 Hz. It leads to a high sensitivity of the impedance model used, which is an approximation of the real experimental acoustic liner. Another possible reason for such a difference in SPL results is that the effect of hydrodynamic instability is not properly taken into account in the One-Way equations, for this specific baseflow profile. Finally, the presence of a non-linear mechanism or the apparition of 3D waves at $f = 3000$ Hz could be at the origin of this discrepancy with experimental data.

In order to reduce these differences in results, we looked at the second type of baseflow profile (turbulent Poiseuille flow), which represents better the experimental baseflow obtained in [30]. We realized a parametric study around n_y to find a relevant value for the OWE and OWNS simulations. We have found that the better compromise for the OWE simulations was $n_y = 5$, as we observed numerical instabilities for larger values of this parameter, resulting in significant increases in SPL from the liner subdomain. We did not manage to prevent these instabilities, even by refining the mesh or adapting $\beta_{\pm}$ coefficients. If the SPL obtained for a frequency of 1500 Hz is closer to the experimental data than in Case 1, the effect of the boundary layer thickness of this baseflow profile is still not sufficient to correctly take the instability into account. The closest results were finally obtained for the OWNS simulations for a n_y value of 7.5, as we also observed numerical instabilities for parameter values above 7.5. For all frequencies tested, the OWNS results in Case 2 were close to the experimental results, in particular for the 1000 Hz frequency where the hydrodynamic instability is well captured. The viscosity contained in the linearized Navier-Stokes equations combined to this baseflow profile may allow us to find better SPL behavior, which was underestimated in all other numerical simulations. However, OWNS results may be improved by considering not only the laminar viscosity, but also the turbulent eddy viscosity, as it has been discussed in [37].

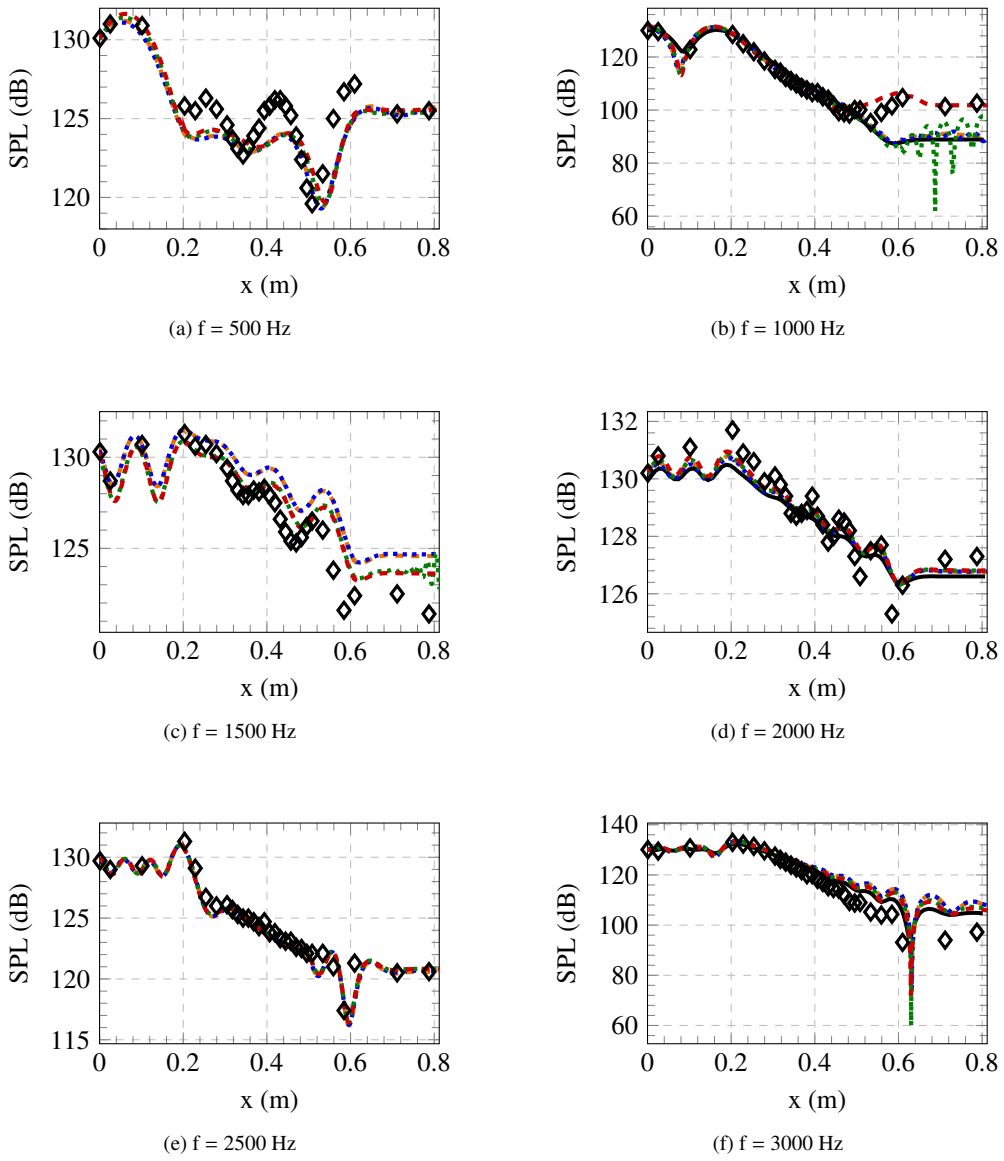

(a) f = 500 Hz

(b) f = 1000 Hz

(c) f = 1500 Hz

(d) f = 2000 Hz

(e) f = 2500 Hz

(f) f = 3000 Hz

Figure 7: Sound Pressure Level (SPL) of the acoustic pressure along the upper wall for different frequencies. Comparison between the experimental data (◇) [30], the mode-matching method (——) [33] and the OW simulations with domain decomposition: OWE (· · · · ·) for Case 1, OWE for Case 2 (· · · · ·), OWNS (- - -) for Case 1 and OWNS for Case 2 (- - -).

4.3.2. Analysis of acoustic liners' performance by the construction of the scattering matrix

One of the particular feature of the One-Way equations is that it is possible to naturally decompose the result obtained into the right and left-going contributions everywhere inside the computational domain. The SPL of these two contributions and the final OWNS results are presented in Figure 8 for Case 2 with a 1000 Hz frequency. As expected, the SPL of the right-going

part remains constant in the inlet domain. After the first discontinuity, the SPL starts to decrease before settling at a certain value with damped oscillations. At the bottom, oscillations are generated by the liner that correspond to the surface wave, which tends to be unstable depending on the baseflow profile. These oscillations grow in amplitude inside the liner domain before getting simply convected when the wave crosses the second interface between the liner and the outlet domain. Concerning the left-going contribution, special care must be taken for its interpretation since a different color scale is used compared to the other two plots. The SPL of the left-going part is not available in the outlet domain, since no left propagating wave is present inside this domain. Therefore, the SPL value presented inside the liner domain comes from the reflection of the right-going incident wave and decreases in value along the liner without any instability. In the inlet domain, the transmission of the left-going wave from the liner domain and the reflection of the right-going wave is propagated with a fixed SPL value without any disturbance. Finally, the sum of both contributions is presented at the bottom and does not present any discontinuity at the interfaces between domains. The fact that this result is continuous even across the interfaces is an indication about the good approximation of the pseudo-eigenvectors matrices used for the projection and the good convergence of the iterative process used for the domain decomposition.

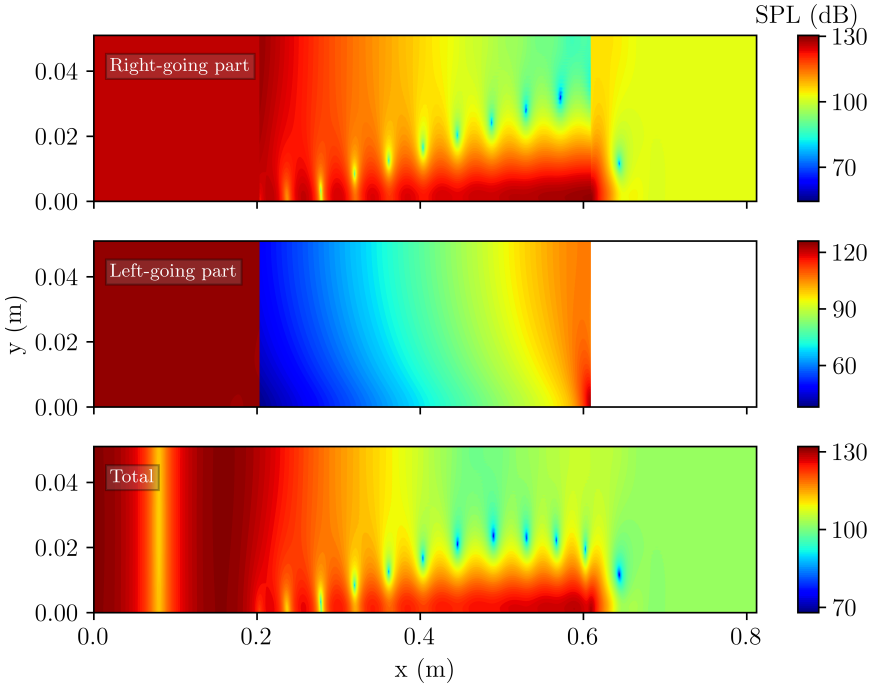

Figure 8: Decomposition of the SPL into the right- and left-going components and total OWNS results for Case 2 at a frequency of 1000 Hz.

Having access to this decomposition into left-going and right-going components provides direct access to the scattering matrix that is used to evaluate the performance of acoustic liners [38, 39] and other configurations [40, 41]. This scattering matrix can be expressed in the

following relation:

$$\begin{pmatrix} p_+^3 \\ p_-^1 \end{pmatrix} = \begin{pmatrix} S_{++} & S_{+-} \\ S_{-+} & S_{--} \end{pmatrix} \begin{pmatrix} p_+^1 \\ p_-^3 \end{pmatrix}, \tag{69}$$

where p_+^1 and p_-^1 are the values of pressure perturbations of the right and left propagating waves at the inlet, while p_+^3 and p_-^3 are the values of pressure perturbations of the right and left propagating waves at the outlet of the duct. The coefficients S_{++} and S_{--} can be seen as the transmission coefficients of the right and left-going waves in this particular duct, while S_{+-} and S_{-+} can be interpreted as the reflection coefficients of the right and left-going incident waves in this duct.

The modulus of these scattering coefficients obtained, depending on the frequency, for this particular lined duct and for the baseflow profile used in Case 2 are plotted in Figure 9. The data obtained for S_{++} and S_{-+} comes directly from the simulations presented previously. These other simulations have been carried out with the same parameters as explained before, with a 130 dB plane wave mode imposed at the inlet (left source). However, to obtain the values of S_{--} and S_{+-}, another set of simulations has been computed with a left-going plane wave mode used as initialization and imposed at the outlet of the duct (right source) with the same SPL of 130 dB. The value of the pressure from the left- and right-going waves at the inlet and outlet have been averaged transversely for the computation of the scattering coefficients.

Concerning the right propagating incident wave (Figures 9a and 9c), as expected, the transmission coefficient S_{++} is very low for 1000 Hz values and OWE results. The overestimation of this wave damping for a left source can be explained by the fact that the OWE equations do not correctly capture the effect of the hydrodynamic instability, as shown above in the SPL results. Moreover, at the same frequency, the reflection coefficient S_{-+} shows a peak, indicating that a significant part of the incident wave is reflected through the duct inlet. Furthermore, the choice of equation model (OWE or OWNS) does not seem to have any influence on the value of this reflection coefficient.

When a wave is propagated upstream across this section of the liner (Figures 9b and 9d), the diffusion coefficient S_{--} behaves in the same way as the other transmission coefficient S_{++}, but with lower values. The evolution of the reflection coefficient S_{+-} closely resembles the other reflection coefficient computed in the opposite direction with a left source. The main difference is that the maximum value is lower, although the peak is still reached for 1000 Hz, for both OWE and OWNS results. The fact that the scattering coefficients are smaller in this direction than in the other may suggest that the acoustic liner acts more effectively on waves propagating upstream than downstream.

All these explanations being assumptions, further studies are needed in the future. In order to confirm or refute them, more in-depth researches are required and the One-Way equations could prove to be a good tool allowing us to decompose and elucidate these complex phenomena.

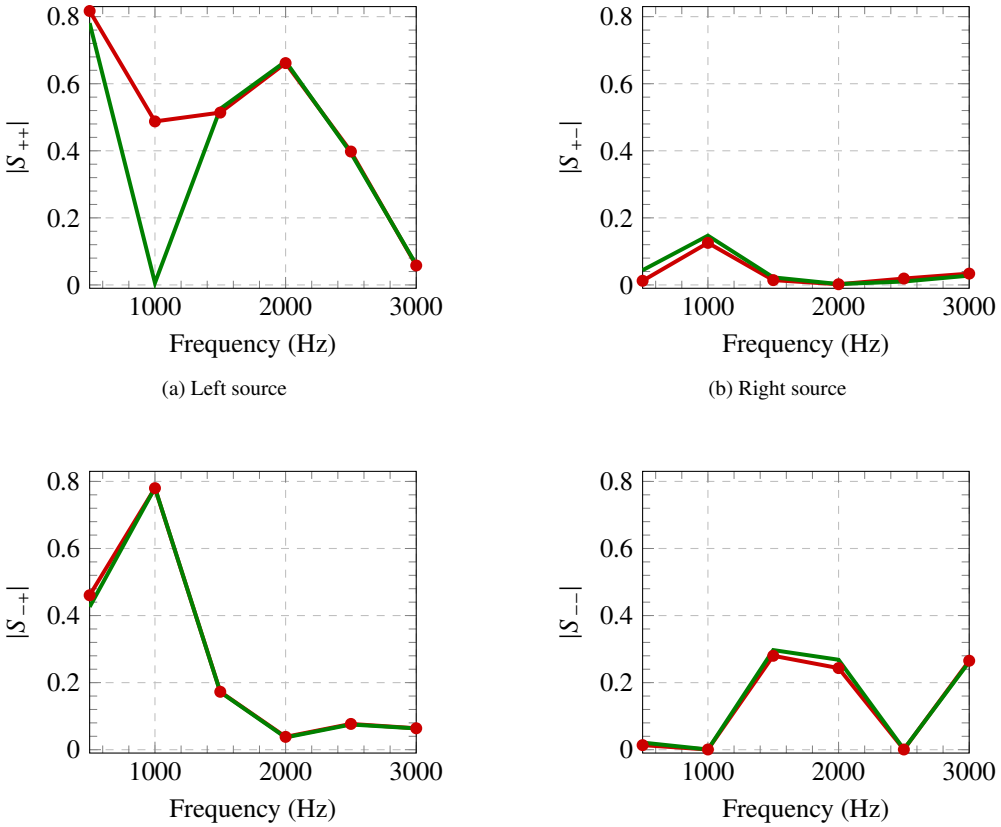

(a) Left source

(b) Right source

(c) Left source

(d) Right source

Figure 9: Coefficients of the partially lined duct's scattering matrix for the OWE (——) and the OWNS results (—●—) in Case 2.

5. Conclusion

The OWE and OWNS equations are coupled with a domain decomposition method that is directly derived from the numerical factorization performed to separate the right- from the left-going waves inside the One-Way equations. This methodology is applied here to a case of partially lined duct, where the discontinuity in boundary conditions (hard-wall and impedance boundary conditions) leads to the generation of reflected and transmitted waves propagating in both directions. A process of iterative One-Way resolutions is then applied to retrieve a full wave result after convergence.

In particular, this method is applied to a case presenting a sheared baseflow throughout the lined duct. This example presented is studied with two different profiles, with various boundary layer thicknesses and with linearized Euler or Navier-Stokes equations. The comparison between the OWE and OWNS simulations show little to no difference in SPL results for almost all frequencies, with one exception for the case which presents a hydrodynamic instability. For this special frequency, the OWNS simulation with the second type of baseflow shows a better

accordance with the experimental data than the one with the first baseflow or than the two OWE simulations.

Moreover, the natural decomposition of the One-Way result into its left and right-going components allows to directly obtain the scattering matrix of this particular lined duct, which is often used for the characterization of the performance of a lined section. Finally, this decomposition is used to investigate the behavior of the acoustic liner in the case of a right and left-going incident plane wave mode and their respective reflections.

Acknowledgements

This work was partly supported by the French "Programme d'Investissements d'avenir" ANR-17-EURE-0005 conducted by ANR.

Appendix A. Operator matrices

Appendix A.1. Linearized Euler equations

Matrices of the linearized Euler equations, taking into account the specific features of the base flow:

$$A = \begin{pmatrix} \overline{u} & a^2\overline{\rho} & 0 \\ \frac{1}{\overline{\rho}} & \overline{u} & 0 \\ 0 & 0 & \overline{u} \end{pmatrix}; B_y = \begin{pmatrix} 0 & 0 & -a^2\overline{\rho} \\ 0 & 0 & 0 \\ -\frac{1}{\overline{\rho}} & 0 & 0 \end{pmatrix}; C = \begin{pmatrix} 0 & 0 & 0 \\ 0 & 0 & -\overline{u}_y \\ 0 & 0 & 0 \end{pmatrix}. \tag{A.1}$$

The eigenvalue matrix $\widetilde{A}$ is given by the following expression:

$$\widetilde{A} = \begin{pmatrix} \overline{u} + a & 0 & 0 \\ 0 & \overline{u} & 0 \\ 0 & 0 & \overline{u} - a \end{pmatrix}, \tag{A.2}$$

where a is the speed of sound.

Transformation matrices used for the first variable change between the primitive and characteristic variables $q = T\phi$:

$$T = \begin{pmatrix} 1 & 0 & 1 \\ a\overline{\rho} & 0 & -a\overline{\rho} \\ 0 & 1 & 0 \end{pmatrix} \text{ and } T^{-1} = \begin{pmatrix} \frac{1}{2} & \frac{1}{2a\overline{\rho}} & 0 \\ 0 & 0 & 1 \\ \frac{1}{2} & -\frac{1}{2a\overline{\rho}} & 0 \end{pmatrix}. \tag{A.3}$$

Expression of the propagation operator of the linearized Euler equations in this particular case:

$$M(x,y) = \begin{pmatrix} \frac{1}{\overline{u}+a} & 0 & 0 \\ 0 & \frac{1}{\overline{u}} & 0 \\ 0 & 0 & \frac{1}{\overline{u}-a} \end{pmatrix} \begin{pmatrix} i\omega & -\frac{\overline{\rho}a^2}{2}\partial_y - \frac{\overline{u}_y}{2a\overline{\rho}} & 0 \\ -\frac{\partial_y}{\overline{\rho}} & i\omega & -\frac{\partial_y}{\overline{\rho}} \\ 0 & -\frac{\overline{\rho}a^2}{2}\partial_y + \frac{\overline{u}_y}{2a\overline{\rho}} & i\omega \end{pmatrix}, \tag{A.4}$$

with $\overline{u}_y$ being the first derivative in y of the variable $\overline{u}$.

Appendix A.2. Linearized Navier-Stokes equations

Matrices of the linearized Navier-Stokes equations, taking into account the specific features of the base flow:

$$A = \begin{pmatrix} \overline{u} & -\overline{v} & 0 & 0 \\ 0 & \overline{u} & 0 & \overline{v} \\ 0 & 0 & \overline{u} & 0 \\ 0 & \gamma\overline{p} & 0 & \overline{u} \end{pmatrix}, \tag{A.5}$$

$$B_y = \begin{pmatrix} 0 & 0 & -\overline{v} & 0 \\ 0 & 0 & 0 & 0 \\ 0 & 0 & 0 & \overline{v} \\ 0 & -\frac{2(\gamma-1)\mu}{Re}\overline{u}_y & \gamma\overline{p} & 0 \end{pmatrix} \tag{A.6}$$

$$B_{yy} = \begin{pmatrix} 0 & 0 & 0 & 0 \\ 0 & -\frac{\overline{v}}{Re}\mu & 0 & 0 \\ 0 & 0 & -\frac{\overline{v}}{Re}\frac{4\mu}{3} & 0 \\ -\frac{(\gamma-1)k}{RPrRe}\overline{p} & 0 & 0 & -\frac{(\gamma-1)k}{RPrRe}\overline{v} \end{pmatrix} \tag{A.7}$$

$$C = \begin{pmatrix} 0 & 0 & 0 & 0 \\ -\frac{\mu}{Re}\overline{u}_{yy} & 0 & \overline{u}_y & 0 \\ 0 & 0 & 0 & 0 \\ 0 & 0 & 0 & 0 \end{pmatrix} \tag{A.8}$$

The eigenvalue matrix $\widetilde{A}$ is given by the following expression:

$$\widetilde{A} = \begin{pmatrix} \overline{u} + a & 0 & 0 & 0 \\ 0 & \overline{u} & 0 & 0 \\ 0 & 0 & \overline{u} & 0 \\ 0 & 0 & 0 & \overline{u} - a \end{pmatrix}, \tag{A.9}$$

where a is the speed of sound.

Transformation matrices used for the first variable change between the primitive and characteristic variables $q = T\phi$:

$$T = \begin{pmatrix} -\frac{\overline{v}^2}{a^2} & 1 & 0 & -\frac{\overline{v}^2}{a^2} \\ \frac{\overline{v}}{a} & 0 & 0 & -\frac{\overline{v}}{a} \\ 0 & 0 & 1 & 0 \\ 1 & 0 & 0 & 1 \end{pmatrix} \text{ and } T^{-1} = \begin{pmatrix} 0 & \frac{a}{2\overline{v}} & 0 & \frac{1}{2} \\ 1 & 0 & 0 & \frac{\overline{v}^2}{a^2} \\ 0 & 0 & 1 & 0 \\ 0 & -\frac{a}{2\overline{v}} & 0 & \frac{1}{2} \end{pmatrix}. \tag{A.10}$$

Appendix B. Characteristic boundary conditions

Appendix B.1. Linearized Euler equations

Starting from the relation $\widetilde{q} = T\phi$, we have:

$$\begin{cases} \widetilde{p} = \phi_1 + \phi_3 \\ \widetilde{u} = a\overline{\rho}(\phi_1 - \phi_3), \\ \widetilde{v} = \phi_2. \end{cases} \tag{B.1}$$

Hard wall. Since it is possible to discretize the propagation operator in terms of characteristic variables, it is also possible to express the relation (64) in these variables to enforce the hard wall boundary condition. Since this set of equations does not change anything to the diagonalization of the matrix A, the transformation matrices T and T^{-1} are also the same as previously. The same can be said about $\widetilde{A}$ and the eigenvalues of A. Therefore, by applying the same variable change performed for the Euler equations in this case, we obtain a modified propagation operator $\widetilde{M}$:

$$\widetilde{M}(x,y) = \begin{pmatrix} \frac{1}{\overline{u}+a} & 0 & 0 \\ 0 & \frac{1}{\overline{u}} & 0 \\ 0 & 0 & \frac{1}{\overline{u}-a} \end{pmatrix} \begin{pmatrix} i\omega + \frac{Sa}{2}\partial_y & -\frac{\overline{\rho}a^2}{2}\partial_y & \frac{Sa}{2}\partial_y \\ 0 & i\omega & 0 \\ \frac{Sa}{2}\partial_y & -\frac{\overline{\rho}a^2}{2}\partial_y & i\omega + \frac{Sa}{2}\partial_y \end{pmatrix}. \tag{B.2}$$

Acoustic liner.

$$\phi_1 + \phi_3 = Z(\omega)\phi_2 \ . \tag{B.3}$$

This equation is imposed on the second equation which transports ϕ_2 while the other two equations remain unchanged.

Appendix B.2. Linearized Navier-Stokes equations

Starting from the relation $\widetilde{q} = T\phi$, we have:

$$\begin{cases} \widetilde{\nu} = -\dfrac{\overline{\nu}}{\gamma\overline{p}}\phi_1 + \phi_2 - \dfrac{\overline{\nu}}{\gamma\overline{p}}\phi_4, \\ \widetilde{u} = \sqrt{\dfrac{\overline{\nu}}{\gamma\overline{p}}}\phi_1 - \sqrt{\dfrac{\overline{\nu}}{\gamma\overline{p}}}\phi_4, \\ \widetilde{\nu} = \phi_3, \\ \widetilde{p} = \phi_1 + \phi_4, \end{cases} \tag{B.4}$$

with γ the heat capacity ratio taken equal to 1.4.

Hard wall. Equation (65) can be rewritten in terms of characteristic variables:

$$\begin{cases} \phi_1 - \phi_4 = 0, \\ \phi_3 = 0, \\ (1 - \dfrac{1}{\gamma})\phi_1 + \dfrac{\overline{p}}{\overline{\nu}}\phi_2 + (1 - \dfrac{1}{\gamma})\phi_4 = 0. \end{cases} \tag{B.5}$$

Acoustic liner. For the application of the impedance condition to model the behavior of an acoustic liner, Equation (66) can be expressed in characteristic variables under the following form:

$$\phi_1 + \phi_4 = Z(\omega)\phi_3 \ . \tag{B.6}$$

This equation is imposed on the third equation which transports ϕ_3 while the other three equations remain unchanged.

References

[1] C. K. W. Tam, Computational aeroacoustics: A wave number approach, Cambridge University Press, 2012.

[2] Y. Özyörük, L. N. Long, Time-domain calculation of sound propagation in lined ducts with sheared flows, AIAA Journal 38 (5) (2000) 768–773. doi:https://doi.org/10.1006/jcph.1998.5919.

[3] C. K. W. Tam, L. Auriault, Time-domain impedance boundary conditions for computational aeroacoustics, AIAA journal 34 (5) (1996) 917–923. doi:https://doi.org/10.2514/3.13168.

[4] C. Richter, J. A. Hay, N. Schönwald, S. Busse, F. Thiele, A review of time-domain impedance modelling and applications, J. Sound Vib. 330 (16) (2011) 3859–3873. doi:https://doi.org/10.1016/j.jsv.2011.04.013.

[5] F. Monteghetti, D. Matignon, E. Piot, Energy analysis and discretization of nonlinear impedance boundary conditions for the time-domain linearized Euler equations, J. Comput. Phys. 375 (2018) 393–426. doi:https://doi.org/10.1016/j.jcp.2018.08.037.

[6] F. Q. Hu, A perfectly matched layer absorbing boundary condition for linearized Euler equations with a non-uniform mean flow, J. Comput. Phys. 208 (2) (2005) 469–492. doi:https://doi.org/10.1016/j.jcp.2005.02.028.

[7] G. Gabard, Mode-matching techniques for sound propagation in lined ducts with flow, in: 16th AIAA/CEAS Aeroacoustics Conference, 2010, p. 3940. doi:https://doi.org/10.2514/6.2010-3940.

[8] W. Koch, Radiation of sound from a two-dimensional acoustically lined duct, J. Sound Vib 55 (2) (1977) 255–274. doi:https://doi.org/10.1016/0022-460X(77)90598-3.

[9] J. Claerbout, Imaging the Earth's Interior, Blackwell Scientific Publications, 1985. doi:https://doi.org/10.1190/1.1440185.

[10] T. Herbert, Parabolized stability equations, Annual Review of Fluid Mechanics 29 (1997) 245–283. doi:https://doi.org/10.1146/annurev.fluid.29.1.245.

[11] M. Taylor, Pseudo Differential Operators, Vol. 416 of Lecture Notes in Mathematics, Springer, 1974. doi:https://link.springer.com/book/10.1007/BFb0101246.

[12] H. Barucq, B. Duquet, F. Prat, True amplitude One-Way propagation in heterogeneous media, Tech. Rep. 6517, INRIA (2008).

[13] A. Towne, T. Colonius, Continued development of the One-Way Euler equations: application to jets, in: 20th AIAA/CEAS Aeroacoustics Conference, Atlanta, Georgia, 2014, p. 2903. doi:https://doi.org/10.2514/6.2014-2903.

[14] A. Towne, T. Colonius, One-way spatial integration of hyperbolic equations, J. Comput. Phys. 300 (2015) 844–861. doi:https://doi.org/10.1016/j.jcp.2015.08.015.

[15] A. Towne, Advancements in jet turbulence and noise modeling: accurate One-Way solutions and empirical evaluation of the nonlinear forcing of wavepackets, Ph.D. thesis, California Institute of Technology (2016).

[16] R. Higdon, Absorbing Boundary Conditions for Difference Approximation to the Multi-Dimensional Wave Equation, Math. Comput. 47 (176) (1986) 437–459. doi:https://doi.org/10.2307/2008166.

[17] R. Higdon, Numerical Absorbing Boundary Conditions for the Wave Equation, Math. Comput. 49 (179) (1987) 65–90.

[18] D. Givoli, B. Neta, High-order non-reflecting boundary scheme for time-dependent waves, J. Comput. Phys. 186 (2003) 24–46. doi:https://doi.org/10.1016/S0021-9991(03)00005-6.

[19] T. Hagstrom, T. Warburton, A new auxiliary variable formulation of high-order local radiation boundary conditions: corner compatibility conditions and extensions to first-order systems, Wave Motion 39 (4) (2004) 327–338. doi:https://doi.org/10.1016/j.wavemoti.2003.12.007.

[20] C. Rudel, S. Pernet, J.-P. Brazier, Numerical Factorization of Propagation Operator for Hyperbolic Equations and Application to One-way, True Amplitude One-way Equations and Bremmer series, J. Sci. Comput. 93 (27) (2022) 1–40. doi:https://doi.org/10.1007/s10915-022-01985-7.

[21] C. Rudel, S. Pernet, J.-P. Brazier, Backscattering in complex flow: application of the One-Way Euler equations to Poiseuille flow inside lined ducts, in: AIAA Aviation 2021 Forum, 2021, p. 2138. doi:https://doi.org/10.2514/6.2021-2138.

[22] L. Gamet, F. Ducros, F. Nicoud, T. Poinsot, Compact finite difference schemes on non-uniform meshes. Application to direct numerical simulations of compressible flows, Int. J. Numer. Methods Fluids 29 (1999) 159–191. doi:https://doi.org/10.1002/(SICI)1097-0363(19990130)29:2¡159::AID-FLD781¿3.0.CO;2-9.

[23] R. Briggs, Electron-stream interaction with plasmas, MIT Press, 1964.

[24] D. A. Di Pietro, A. Ern, Mathematical Aspects of Discontinuous Galerkin Methods, Vol. 69 of Mathématiques & Applications, Springer, 2012.

[25] F. Collino, S. Ghanemi, P. Joly, Domain Decomposition Method for Harmonic Wave Propagation : A General Presentation, Tech. Rep. 3473, INRIA (1998).

[26] Y. Özyörük, L. N. Long, M. G. Jones, Time-domain numerical simulation of a flow-impedance tube, J. Comput. Phys. 146 (1998) 29–57. doi:https://doi.org/10.1006/jcph.1998.5919.

[27] L. Pascal, E. Piot, G. Casalis, A new implementation of the extended Helmholtz resonator acous-

tic liner impedance model in time domain CAA, J. Comput. Acoust. 24 (01) (2015) 1550015. doi:https://doi.org/10.1142/S0218396X15500150.

[28] G. Rigas, T. Colonius, M. Beyar, Stability of wall-bounded flows using One-Way spatial integration of Navier-Stokes equations, in: 55th AIAA Aerospace Sciences Meeting, 2017, p. 1881. doi:https://doi.org/10.2514/6.2017-1881.

[29] M. Zhu, A. Towne, Recursive One-Way Navier-Stokes equations with PSE-like cost, J. Comput. Phys. 473 (2023) 111744. doi:https://doi.org/10.1016/j.jcp.2022.111744.

[30] M. Jones, W. Watson, T. Parrott, Benchmark data for evaluation of aeroacoustic propagation codes with grazing flow, in: 11th AIAA/CEAS Aeroacoustics Conference, Monterey, California, 2005, p. 2853. doi:https://doi.org/10.2514/6.2005-2853.

[31] C. Richter, F. H. Thiele, M. Zhuang, Comparison of time-domain impedance boundary conditions for lined duct flows, AIAA Journal 45 (6) (2007) 1333–1345. doi:https://doi.org/10.2514/1.24945.

[32] M. O. Burak, M. Billson, L.-E. Eriksson, S. Baralon, Validation of a Time- and Frequency-Domain Grazing Flow Acoustic Liner Model, AIAA Journal 47 (8) (2009) 1841–1848. doi:https://doi.org/10.2514/1.40870.

[33] Y. Deng, D. Dragna, M.-A. Galland, A. Alomar, Comparison of three numerical methods for acoustic propagation in a lined duct with flow, in: 25th AIAA/CEAS Aeroacoustics Conference, Delft, The Netherlands, 2019, p. 2658. doi:https://doi.org/10.2514/6.2019-2658.

[34] A. H. Nayfeh, J. E. Kaiser, D. P. Telionis, Acoustics of aircraft engine-duct systems, AIAA Journal 13 (2) (1975) 130–153. doi:https://doi.org/10.2514/3.49654.

[35] G. Boyer, E. Piot, J.-P. Brazier, Theoretical investigation of hydrodynamic surface mode in a lined duct with sheared flow and comparison with experiment, J. Sound Vib. 330 (2011) 1793–1809. doi:https://doi.org/10.1016/j.jsv.2010.10.035.

[36] D. Marx, Numerical Computation of a Lined Duct Instability Using the Linearized Euler Equations, AIAA Journal 53 (8) (2015) 2379–2388. doi:https://doi.org/10.2514/1.J053746.

[37] D. Marx, Y. Aurégan, Effect of turbulent eddy viscosity on the unstable surface mode above an acoustic liner, J. Sound Vib. 332 (2013) 3803–3820. doi:https://doi.org/10.1016/j.jsv.2013.02.005.

[38] M. Åbom, Measurement of the scattering-matrix of acoustical two-ports, Mech. Syst. Signal Process. 5 (2) (1991) 89–104. doi:https://doi.org/10.1016/0888-3270(91)90017-Y.

[39] M. Taktak, J.-M. Ville, M. Haddar, F. Foucart, Evaluation of the lined duct performances based on a 3D two port scattering matrix, Proc. Mtgs. Acoust. 4 (2008) 157–168. doi:https://doi.org/10.1121/1.2975221.

[40] S. Félix, V. Pagneux, Multimodal analysis of acoustic propagation in three-dimensional bends, Wave Motion 36 (2002) 157–168. doi:https://doi.org/10.1016/S0165-2125(02)00009-4.

[41] M. Merk, C. Silva, W. Polifke, R. Gaudron, M. Gatti, C. Mirat, T. Schuller, Direct Assessment of the Acoustic Scattering Matrix of a Turbulent Swirl Combustor by Combining System Identification, Large Eddy Simulation and Analytical Approaches, J. Eng. Gas Turbines Power. 141 (2019) 021035. doi:https://doi.org/10.1115/1.4040731.